Basic Research in Cardiology (2022) 117:51
https://doi.org/10.1007/s00395-022-00957-0

ORIGINAL CONTRIBUTION

Osteopontin promotes infarct repair

Itai Rotem[1,2] · Tal Konfino[1,2] · Tal Caller[1,2] · Yeshai Schary[1,2] · Olga Shaihov-Teper[1,2] · Dahlia Palevski[1,2] · Nir Lewis[1,2] · Daria Lendengolts[2,3] · Nili Naftali-Shani[1,2,3] · Jonathan Leor[1,2,3]

Received: 30 September 2021 / Revised: 22 September 2022 / Accepted: 23 September 2022 / Published online: 14 October 2022

Abstract

Understanding how macrophages promote myocardial repair can help create new therapies for infarct repair. We aimed to determine what mechanisms underlie the reparative properties of macrophages. Cytokine arrays revealed that neonatal cardiac macrophages from the injured neonatal heart secreted high amounts of osteopontin (OPN). In vitro, recombinant OPN stimulated cardiac cell outgrowth, cardiomyocyte (CM) cell-cycle re-entry, and CM migration. In addition, OPN induced nuclear translocation of the cytoplasmatic yes-associated protein 1 (YAP1) and upregulated transcriptional factors and cell-cycle genes. Significantly, by blocking the OPN receptor CD44, we eliminated the effects of OPN on CMs. OPN also activated the proliferation and migration of non-CM cells: endothelial cells and cardiac mesenchymal stromal cells in vitro. Notably, the significant role of OPN in myocardial healing was demonstrated by impaired healing in OPN-deficient neonatal hearts. Finally, in the adult mice, a single injection of OPN into the border of the ischemic zone induced CM cell-cycle re-entry, improved scar formation, local and global cardiac function, and LV remodelling 30 days after MI. In summary, we have shown, for the first time, that recombinant OPN activates cell-cycle re-entry in CMs. In addition, recombinant OPN stimulates multiple cardiac cells and improves scar formation, LV remodelling, and regional and global function after MI. Therefore, we propose OPN as a new cell-free therapy to optimize infarct repair.

Keywords Cardiomyocyte · Cell cycle · Myocardial infarction · Macrophage · Osteopontin

Introduction

Understanding the mechanism of myocardial regeneration and repair can facilitate the efforts to develop new therapies for myocardial injury. However, despite extensive research [18, 44], a clinically relevant treatment to regenerate or repair the human heart has not been found [14, 43].

Introducing the neonatal mouse model of transient myocardial regeneration enables new opportunities to investigate the process of myocardial regeneration and repair [17, 42]. These studies identified several factors that may promote CM proliferation to regenerate adult mammalian hearts [14, 18, 44, 58].

Macrophages are essential for infarct repair and myocardial rejuvenation [2, 6, 13, 26, 45]. The ability of macrophages to penetrate injured tissues, integrate environmental signals and transmit regenerative mediators position these cells as central orchestrators of the reparative process. Therefore, studies on how macrophages control myocardial rejuvenation could identify pathways and molecules that may promote myocardial repair (regeneration or healing) in the adult heart.

Here, we sought to determine what underlies the reparative properties of macrophages in neonatal and adult hearts. We identified a significant role of the matricellular protein osteopontin (OPN) in infarct repair and CM cell-cycle re-entry. Thus, we propose that OPN can be used as a new reparative agent to improve infarct repair.

Itai Rotem and Tal Konfino have equal contribution.

✉ Jonathan Leor
leorj@tauex.tau.ac.il

[1] Faculty of Medicine, Neufeld Cardiovascular Research Institutes, Tel Aviv University, Tel-Aviv, Israel

[2] Tamman Cardiovascular Research Institutes, Sheba Medical Center, 52621 Tel-Hashomer, Israel

[3] The Leviev Cardiovascular and Thoracic Center, Sheba Medical Center, Tel-Hashomer, Israel

Methods

The authors declare that all supporting data are available within the article and its online supplementary files. More data supporting this study's findings are available from the corresponding author upon reasonable request.

Our study has been approved by the Sheba Medical Center Internal Review Board Committee and was performed following the guidelines of the Animal Care and Use Committee of the Sheba Medical Center and Tel Aviv University.

Animals

Wild-type C57BL/6 and ICR mice were purchased from Envigo RMS (Jerusalem, Israel).

To assess monocyte/macrophage accumulation in the neonatal heart, we used macrophage reporter $Rosa^{mt/mg}$ × Csf-1R-iCre neonatal mice [37]. We crossed Csf-1R-iCre mice with the Cre-reporter [34] $Rosa^{mt/mg}$ [11] mice, in which Csf-1R-positive cells are GFP-positive.

$OPN^{\pm}$ C57BL/6 mice were supplied courtesy of Prof. Eli Pikarsky, Hadassah Medical Center, Jerusalem. The mice were crossed to generate homozygote knockout ($OPN^{-/-}$) and controls (C57BL/6 WT). In all mouse experiments, WT littermates were used as controls. To confirm genotypes, we cut the tips of mouse tails, and DNA was extracted with direct PCR solution (Viagen Biotech, Los Angeles, California, USA) and Proteinase K (Roche Diagnostics GmbH, Mannheim, Germany).

Neonatal mouse model of apical resection (AR) or myocardial infarction (MI)

To determine the role of macrophages in myocardial regeneration and repair, we used a neonatal mouse model of AR or MI [30]. One-day-old neonatal ICR mice (Envigo RMS, Jerusalem, Israel) were subjected to AR, MI, or sham operation ($n=30$). To avoid pain and stress, we anesthetized newborn mice by inhaling 2% isofluorane and 100% oxygen. Then, the mice were cooled down on an ice bed for 4 min, causing asystole and reversible apnea [40] and preventing excessive blood loss during surgery. The cooling-down period also provided additional anesthesia.

To perform AR, we opened the chest by left thoracotomy and used iridectomy scissors to carefully and gradually resect thin segments from the left ventricular (LV) apex, as previously described [22, 30, 42]. Then, the thoracic skin was closed using adhesive tissue glue [30].

We used a similar surgery protocol to induce MI in neonatal mice [2, 22, 30]. MI was induced by permanent occlusion of the mid-left anterior descending (LAD) coronary artery by an 8-0 prolene suture (Ethicon, Cornelia, GA, USA) [2, 22, 30]. After MI, animals were placed on a heating pad (37 °C), allowed to recover, and returned to their mothers. Sham-operated mice underwent the same procedure without AR or MI. The average survival rate in neonatal mice after AR and MI was 70% and 40%. Survival after the sham operation was 95%.

The area of inflammation and granulation tissue 3 days post AR ($n=5$ for WT, $n=4$ for OPN KO) was measured using SigmaScan Pro 5 (Systat Software San Jose, CA, USA).

MI in adult mice

To determine the role of OPN in infarct repair, we used the mouse model of MI in female 12-week-old ICR mice (Envigo RMS, Jerusalem, Israel) [6, 22, 35, 37]. Mice were anesthetized with 1–3% isofluorane, intubated, and ventilated with 100% oxygen. The chest was shaved and opened by left thoracotomy, and LAD ligation was performed using an 8-0 Prolene suture (Ethicon, Cornelia, GA, USA) to permanently occlude the LAD coronary artery.

In the LV remodelling studies, 40 µl of PBS with or without 200 ng of OPN (O2260, Sigma-Aldrich, St. Louis, MO, USA) were injected into the border of the ischemic area. Myocardial ischemia was confirmed by visual blanching distal to the occlusion site with wall-motion akinesis [25]. We also confirmed MI by echocardiography 24 h after surgery. The chest was closed, and the skin was sutured with a 5-0 Prolene suture (Ethicon, Cornelia, GA, USA). Mice were placed on a heating pad (37 °C) until recovery. After MI, the average survival rate was 80%, and the average survival rate after the sham operation was 95%.

Cardiac macrophage isolation and culture

Macrophages were purified based on plastic adherence and resistance to trypsinization [6, 37]. We harvested neonatal hearts 3 days after AR, MI, or sham procedure ($n=4$ in each group). We also collected adult macrophages 3 days after MI in the adult mouse ($n=4$). Briefly, cells were incubated for 2 h at 37 °C in humid air with 5% CO_2 on 6-well plates supplemented with RPMI (Biological Industries, Beit-Haemek, Israel) with 10% FBS (Fetal Bovine Serum) (Biological Industries, Beit-Haemek, Israel) and 1% streptomycin. Then, non-adherent cells were washed, and to further ensure macrophage enrichment, 3-min trypsin–EDTA (Ethylenediaminetetraacetic acid) treatment was added to the remaining cells. The trypsin was then blocked with fresh medium and washed, and the intact adherent cells were considered cardiac macrophages. To determine purification efficiency, we stained the cells with the macrophage marker F4/80. We

found > 90% positive staining for F4/80 in culture [37]. Cardiac macrophages were grown for 24 h, and the conditioned medium was collected.

Quantification of macrophage cytokines and chemokines

To detect and quantify macrophage-derived cytokines and chemokines, we collected cell culture supernatant for a custom-made mouse Quantibody Array Kit (RayBiotech Inc. Insight Biotechnology Ltd, Wembley, UK), according to the manufacturer's instructions. The array was designed to quantitatively detect 14 cytokines, chemokines, and growth factors simultaneously: interleukin (IL)-1ß, IL-4, IL-6, IL-10, IL-12 p40/p70, IL-17, monocyte chemoattractant protein (MCP)-1, tumor necrosis factor (TNF)-α, stromal cell-derived factor (SDF)-1, IL-13, vascular endothelial growth factor-A (VEGF-A), insulin-like growth factor (IGF), hepatocyte growth factor (HGF), and osteopontin (OPN). The signals (green fluorescence, Cy3 channel, 555 nm excitation, and 565 nm emission) were captured using a GenePix 4000B laser scanner (Bio-Rad Laboratories, Hercules, CA, USA) and extracted with GenePix Pro 6.0 microarray analysis software. Quantitative data analysis was performed using the RayBiotech mouse Array software (Q-Analyzer Software for QAM-INF-1, Norcross, GA, USA). Sample concentrations (pg/ml) were determined from mean fluorescent intensities (median values) compared with five-parameter linear regression standard curves generated from standards provided by the manufacturer. A series of isochronal maps reflecting the cytokine/chemokine concentrations detected by the microarrays were constructed by Matlab software (R2009a, MathWorks, Inc., Natick, MA, USA) to transform numerical data into simplex graphical patterns.

Organ culture of neonatal hearts

To determine the effect of OPN on neonatal hearts, we used an organ culture [8, 22]. Hearts were harvested from 1-day-old neonatal mice. The atrial area was removed, and the ventricular area was cut into 2 transverse slices cultured on a coated 48-well dish with CM growth media for 48 h to achieve adhesion. Next, tissues were treated with 800 ng/ml OPN (Sigma-Aldrich, St. Louis, MO, USA) or control culture media without OPN (6 wells in each group) for 72 h [50]. Cardiac tissue growth was then assessed by cell budding (outgrowth) from the cultured heart slices using SigmaScan Pro 5 (Systat Software San Jose, CA, USA). The outgrowth was stained with antibodies against α-cardiac actin (Santa Cruz Biotechnology, Dallas, TX, USA), phosphohistone 3 (pH3) (S10 Epitomics, Burlingame, CA, USA), CD31 (Santa Cruz Biotechnology, Dallas, TX, USA), and F4/80 (BioLegend, San Diego, CA, USA).

Isolation and culture of neonatal cardiomyocytes (nCMs)

To explore the effects of OPN on CMs, we isolated and cultured mouse nCMs as previously described [12]. Briefly, hearts ($n = 10$) were extracted from one-day-old mice into a bacterial dish containing PBS. After removing unwanted tissue, the hearts were transferred to a drop of isolation medium (BDM: Sigma-Aldrich, B-0753; HBSS: BI02-017-1B; trypsin 0.25%, Gibco) and minced into small pieces. The pieces were then transferred to a conical tube containing 10 ml of isolation medium and incubated overnight with gentle agitation at 4 °C. Next, the isolation medium was replaced by a digestion medium (collagenase/dispase: Sigma-Aldrich, 10269638001; L-15: BI, 01–115-1A, BDM, HBSS), and the conical tube was transferred to a 37 °C water bath for 20 min with gentle agitation. Then, when the digestive tissue sank to the bottom, supernatant-containing cells were transferred to a fresh conical tube and filled with medium-free collagenase/dispase through a sterile cell strainer (100 µm nylon mesh). After centrifugation, cells taken from the sediment were re-suspended with a plating medium (DMEM high glucose; M-199: BI, 01-080-1B; Horse serum/HS, FBS, pen/strep) and seeded on a 3.5-cm bacterial dish for 2.5 h. Next, the cells were counted after using trypan blue staining for dead cells. The cells (2×10^4/well in a 96-well plate) were plated for 18 h on a 96-well plate pre-coated with collagen 0.01%. Then, we replaced the plating medium with a medium without serum (DMEM low glucose, M-199, pen/strep) and treated the cells with or without 800 ng/ml OPN (O2260, Sigma-Aldrich) for 24 h.

MTT colorimetric assay

To determine the effect of OPN on the number of cardiac cells in culture, we treated nCMs with or without 800 ng/ml OPN (O2260, Sigma-Aldrich) and 10 µg/ml CD44i (KM81, Abcam, Cambridge, UK), an antibody against CD44, for 24 h. Then, the cells were exposed to a 3-(4,5-dimethylthiazol-2-yl)-2,5-diphenyltetrazolium bromide (MTT) colorimetric assay according to the manufacturer's protocol (ab211091, Abcam, Cambridge, UK). Finally, the number of cells was determined using a spectrophotometer with a wavelength of 595 nm.

RealTime-Glo assay

To confirm the effect of OPN on cell number and growth, we used Promega's RealTime-Glo™ MT Cell Viability Assay protocol (Cat.# G9711, Promega, Madison, WI, USA). Briefly, Real Time-Glo reagents were added to nCMs with a low glucose medium without serum and incubated at 37 °C and 5% CO_2 for 1 h. At time 0, luminescence was measured

using a luminometer with an integration time of 0.3 s per well. After adding 800 ng/ml/well of OPN, the cells were returned to the cell culture incubator for 24 h, and luminescence was measured again. The number of cells was calculated by using the average OD (Optical Density) value of 2×10^4 cells at time 0 h, which is the number of seeded cells. This average OD was used as a reference: (24 h OD value/average 0 h OD value) $\times 2\times10^4$ cells = number of cells.

RNA extraction and quantitative RT-PCR (qRT-PCR)

Gene expression analysis in cultured CMs was done by quantitative RT-PCR (qRT-PCR). Total RNA was extracted from nCMs using the RNeasy Mini Kit (Qiagen, Hilden, Germany) according to the manufacturer's protocol. The cDNA was generated from total RNA using the Verso cDNA kit (Thermo Scientific). qRT-PCR was performed in triplicate using absolute blue SYBR Green (Thermo, Waltham, MA, USA). $2^{-\Delta\Delta Ct}$ values were normalized to GAPDH. Statistical analysis was performed using an unpaired t-test. Primers were designed with PMC—NCBI, Primer3 input, and UCSC In-Silico PCR (Supplementary Information Table S1).

nCMs staining

To stain the cultured CMs for various markers, we washed and fixed the CMs using 4% formalin. Blocking (for non-specific sites) was performed using CAS-Block (008120, life technologies, Frederick, MD, USA) for 10 min and MOM (MKB-2213, Burlingame, CA, USA) for 20 min. Next, we used primary antibodies against Actinin (1:200, A7811, Sigma-Aldrich, St. Louis, MO, USA) and pH3 (1:100, S10, ab47297, Abcam, Cambridge, UK) or CD44i (1:100, KM81, ab112178, Abcam, Cambridge, UK) or YAP (1:50, LS-C331201, LSBio, Seattle, WA, USA) for overnight in 4 °C. Then, secondary antibodies Alexa Fluor 488 (1:200, Jackson ImmunoResearch, Cambridge, UK), Texas Red (1:200, Jackson ImmunoResearch, Cambridge, UK), and DAPI (BAR-NAOR, Petah Tikva, Israel) were added.

The ratio of nuclear to cytoplasmic YAP

To determine the extent of nuclear translocation of YAP, we quantified the ratio of nuclear YAP to cytoplasmatic YAP. First, we treated nCMs with or without 800 ng/ml OPN (O2260, Sigma-Aldrich) or 800 ng/ml OPN with 10 µg/ml CD44i (KM81, Abcam, Cambridge, UK), an antibody against CD44, for 24 h. After fixation, we used antibodies against actinin (Green), YAP (Red), and DAPI (Blue). Next, we obtained microscopy images of each well, two wells per treatment group, 4 images per well. Then, we analyzed images using a macro-based algorithm in ImageJ 1.52p (Wayne Rasband, NIH, Bethesda, Maryland, USA) [48, 49]. Briefly, the algorithm recognizes the stained areas for each label, then calculates the fluorescent intensity per label. Finally, we calculated the ratio of YAP (red) staining in the nucleus (blue) to YAP staining in the cytoplasm (green).

Isolation and culture of neonatal cardiac mesenchymal stromal cells (MSCs)

Cardiac MSCs were extracted from neonatal hearts ($n=4$) using an enzymatic digestion mixture containing 0.25% trypsin–EDTA (Gibco-Invitrogen, Carlsbad, CA, USA) and 2.4 U/ml dispase II (Sigma-Aldrich, St. Louis, MO, USA) [35]. Next, the cells were counted using trypan blue and plated with fibroblasts medium (DMEM high-glucose, FBS, pen/strep, glutamine, and β-mercaptoethanol) to 2×10^5 cells/well in a 96-well plate.

Isolation and culture of cardiac macrophages

Cardiac macrophages were extracted from adult mice hearts 3 days after MI ($n=3$ for WT, $n=6$ for OPN KO) using an enzymatic digestion mixture containing 0.25% trypsin–EDTA (Gibco-Invitrogen, Carlsbad, CA, USA) and 2.4 U/ml dispase II, (Sigma-Aldrich, St. Louis, MO, USA) [35]. Next, the cardiac cells were seeded in a 6-well plate and incubated at 37 °C. After 2.5 h, we added trypsin to remove non-macrophage cells, and then macrophage medium [RPMI, 10% FBS, Pen-Strep-Ampho (Biological Industries, Beit-Haemek, Israel)] for overnight incubation. Next, we added a macrophage medium without FBS phenol red for 24 h.

"Wound Healing" scratch assay

To determine the effect of OPN (800 ng/ml) or macrophage conditioned medium on nCMs or MSCs migration and "wound healing", we used the scratch assay [28]. The assay employed a "scratch" across the middle of the well, using a sterile 10 µl pipette tip. Serial microscopy images monitored the rate of gap closure. The images were then compared to quantify the migration rate of the cells.

Endothelial cell (EC) tube formation assay

To determine the effect of OPN on angiogenesis, we used an EC tube formation assay. Basement membrane matrix (Matrigel®, BD Biosciences) was added to a 96-well plate and solidified by incubation at 37 °C for 30 min. Next, 3×10^4 human umbilical vein endothelial cells (HUVECs) were plated onto each Matrigel-containing well with endothelial cell growth medium and with or without 200, 400, or 800 ng/ml/well OPN. Microscopy images of each

well and the amount and structure of the tubes were captured and evaluated after two hours.

Effect of OPN on LV remodelling and function

To determine the effect of OPN on LV remodelling and function, we used 12-week-old female C57BL/6 mice. MI was induced as described above [6, 22, 35, 37]. MI was confirmed by visual blanching distal to the occlusion site and by echocardiography 24 h after MI. Mice were treated with a single injection of 40 µl of PBS with or without 200 ng of recombinant OPN (O2260, Sigma-Aldrich, St. Louis, MO, USA) to the border of the ischemic zone one minute after coronary artery ligation. The dose of OPN was determined based on preliminary toxicity studies and previous reports [1, 9, 56]. Mice with LV ejection fraction > 40% on day 1 after MI were excluded from the study ($n = 15$).

Echocardiography to evaluate cardiac remodelling and function

To assess LV remodelling and function after MI, we used a special small animal echocardiography system (Vevo 2100 Imaging System; VisualSonics, Toronto, Ontario, Canada) equipped with a 22- to 55-MHz linear-array transducer MS550D MicroScan Transducer (VisualSonics, Toronto, Ontario, Canada). Echocardiographic studies were done before, 1, and 28 days after injury or sham operation. Light anesthesia was induced by inhalation of 2% isoflurane/98% O_2 and subsequently maintained by 0.5% to 1% isoflurane. We controlled the isoflurane flow to maintain the heart rate at > 400 bpm (mean 428 ± 8 bpm). All measurements were averaged for 3 consecutive cardiac cycles and performed by an experienced technician blinded to the treatment groups. LV ejection fraction (EF) values were calculated for each animal as follows: LVEF = [(LV vol d-LV vol s)/LV vol d] × 100; fractional shortening = [(LVDD − LVSD)/LVDD] × 100.

To improve the sensitivity to detect regional wall motion abnormalities in adult mice after MI, we used speckle-tracking-based strain analysis to quantify strain in the long and short axes [5, 6]. Echocardiographic images were acquired at 310 and 405 frames per second for parasternal long-axis and short-axis views. Three consecutive cardiac cycles were selected, and the endocardial and epicardial borders were traced. If needed, borders were corrected to preserve as precise tracking as possible throughout each cine loop. Each LV image on the long axis was divided into six segments for regional speckle-tracking-based strain analysis: anterior-base, anterior-middle, anterior-apex, posterior-apex, posterior-middle, and posterior-base. Peak strain data were recorded from each segment for regional speckle-tracking-based strain analysis. The global strain of LV was calculated as the average peak strain obtained from all six segments [5, 6].

Histological and morphometric analysis of the hearts

To assess the cardiac injury, healing, repair, and regeneration after AR, MI, or sham operation, we harvested the hearts at different time points after the procedure and washed them with PBS. The hearts were perfused with 4% formaldehyde (15 mmHg) for 20 min, and measurements were performed on slices obtained 5 mm from the apex of the heart. Adjacent blocks were embedded in paraffin and sectioned into 5 µm slices.

According to standard procedure, we used hematoxylin and eosin (Sigma-Aldrich, St. Louis, MO, USA) for cells and extracellular matrix staining. We used picrosirius red (Direct Red 80, Sigma-Aldrich, St. Louis, MO, USA) to detect scarring and fibrosis. To identify nCM proliferation and macrophage accumulation, we stained heart sections with antibodies against α-cardiac actin (Santa Cruz Biotechnology, Dallas, TX, USA), actinin (Sigma-Aldrich, St. Louis, MO, USA), and pH3 (PS10 Epitomics, Burlingame, CA, USA).

Postmortem morphometric analysis was performed on hearts from the adult MI experiment, as previously described [25]. The slides were stained with hematoxylin and eosin or picrosirius red, photographed and analyzed with planimetry software (Sigma Scan Pro 5, Systat Software, San Jose, California, USA). We measured LV maximal diameter, defined as the longest diameter perpendicular to a line connecting the insertions of the septum to the ventricular wall. We also measured average wall thickness from 3 measurements of septum thickness, average scar thickness from 3 measurements of scar thickness, LV muscle area (including the septum), LV cavity area, whole LV area, epicardial scar length (millimeters), and endocardial scar length (millimeters). Relative scar thickness was calculated as average scar thickness divided by average wall thickness. The expansion index was calculated as follows: [LV cavity area/whole LV area]/relative scar thickness.

Statistical analysis

Statistical analysis was performed with GraphPad Prism version 9.00 (GraphPad Software). Variables are expressed as mean ± SD. Specific statistical tests are detailed in the figure legends. In brief, differences between values were tested by unpaired *t*-test or one-way analysis of variance (ANOVA) test (> 2 groups) followed by Tukey's multiple comparisons post-test. If values were not normally distributed (tested by the D'Agostino-Pearson omnibus normality test), we used the nonparametric Mann–Whitney test or

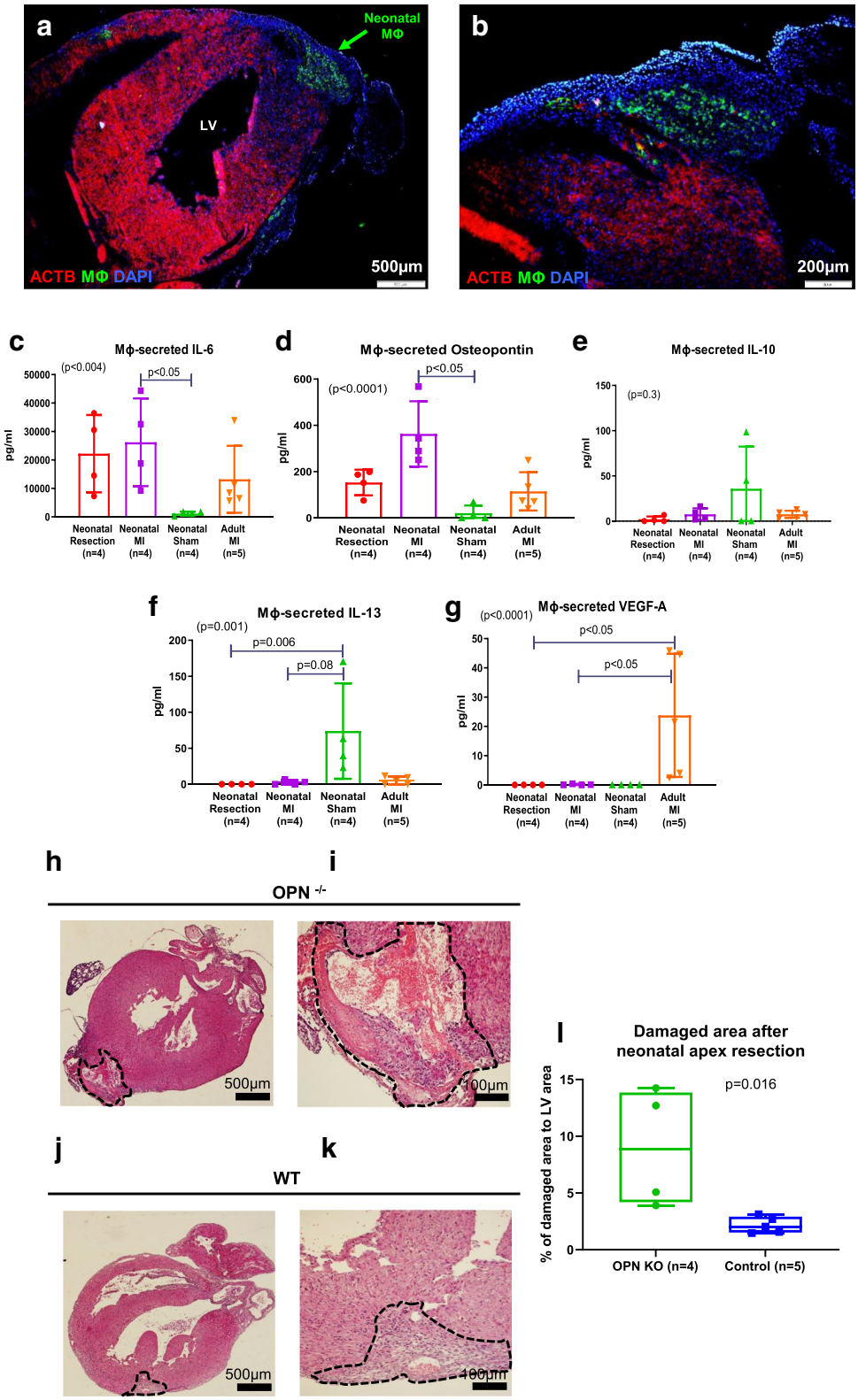

Kruskal–Wallis test (> 2 groups), followed by Dunn's multiple comparisons post-test. Fisher's exact test compared the survival rate in neonatal mice. To assess differences in cardiac function over time, with and without OPN therapy, we used two-way repeated-measures ANOVA followed by Holm-Šídák's multiple comparisons post-test to determine the significance of predefined comparisons at specific time points.

◂**Fig. 1** Macrophages infiltrated the site of injury in the neonatal heart. To explore the role of macrophages in neonatal heart regeneration, we used transgenic $Rosa^{mt/mg}$ × Csf-1R-iCre mice ($n=10$). In these mice, macrophages are marked by green fluorescent protein (GFP) and CMs by tomato red. Then, we induced AR in 1-day-old $Rosa^{mt/mg}$ × Csf-1R-iCre mice (1-day-old) and examined the hearts 3 days later. **a** Monocytes and macrophages (green) accumulated in the injured site, and a thrombus covered the area of resection (arrow). Nuclei are stained blue with DAPI. CM (red) expressed ACTB (β actin). Scale bar: 500 µm. **b** Higher magnification of (**a**). Monocytes and macrophages (green) accumulated at the site of injury but not in remote areas. Nuclei are stained blue with DAPI. CM (red) expressed ACTB. Scale bar: 200 µm. **c–g** Cytokine secretion from cardiac macrophages, 3 days after apical resection, MI, or sham operation in neonatal heart and adult hearts after MI. Macrophages were cultured for 24 h, and conditioned media were analyzed for macrophage-secreted cytokines by Quantibody array. **h–l** To determine the role of OPN in myocardial regeneration, we subjected one-day-old newborn $OPN^{-/-}$ mice ($n=150$) and WT control ($n=51$) C57BL/6 neonatal mice to AR. Healing and repair were determined on day 3 after AR. **h–i** Histologic examination of $OPN^{-/-}$ hearts on day 3 after AR, revealed immature granulation tissue with large cavities (arrow) and incomplete healing ($n=4$). **j–k** Intensive healing and dense granulation tissue (arrow) in the neonatal WT control heart ($n=5$). **l** We used SigmaScan Pro 5 (Systat Software San Jose, CA, USA) to measure the area of injury. Statistical analysis was performed using one-way ANOVA, with Tukey's multiple comparison post-test. *ACTB* β-actin, *AR* apex resection, *DAPI* 4′,6-diamidino-2-phenylindole, *IL* interleukin, *LV* left ventricular, *MI* myocardial infarction, *MΦ* macrophage, *OPN* osteopontin, $OPN^{-/-}$ osteopontin knockout, *VEGF* vascular endothelial growth factor, *WT* wild type

Results

To demonstrate macrophage accumulation in the injured neonatal heart, we used transgenic $Rosa^{mt/mg}$ × Csf-1R-iCre mice ($n=10$). The survival rate after AR was 20%. Next, we used ICR mice to characterize cardiac-macrophage cytokine secretion ($n=78$). In these experiments, the average survival rate in neonatal mice after AR and MI was 40% and 70%. Survival after the sham operation was 95%.

Monocytes and macrophages infiltrated the site of injury in neonatal hearts

Given the results of previous reports indicating that macrophages are essential for myocardial regeneration in the neonatal heart [2, 13, 22, 26], we sought further to understand the role of macrophages in neonatal heart regeneration. First, we resected the apex of $Rosa^{mt/mg}$ × Csf-1R-iCre newborn mice ($n=10$), in which monocytes and macrophages expressed GFP [37]. Three days after AR, a microscopic examination revealed a robust accumulation of monocytes at the large thrombus that covered the resection site and the granulation tissue (Fig. 1a, b).

Neonatal macrophages secreted high amounts of OPN after cardiac injury

Given that macrophages promote myocardial rejuvenation via secreted factors [2], we analyzed the profile of cytokines secreted from cardiac macrophages. First, macrophages were collected from neonatal hearts after AR ($n=7$), MI ($n=10$), or sham operation ($n=5$) 3 days after surgery [6, 37]. Next, we isolated macrophages from adult hearts ($n=5$) 3 days after MI. To determine the macrophage cytokine profile in the regenerating heart, we used a cytokine array of 14 known cytokines: interleukin (IL)-1ß, IL-4, IL-6, IL-10, IL-12 p40/p70, IL-17, monocyte chemoattractant protein (MCP-1), tumor necrosis factor (TNF)-α, stromal cell-derived factor (SDF)-1, IL-13, vascular endothelial growth factor-A (VEGF-A), insulin-like growth factor (IGF), hepatocyte growth factor (HGF), and OPN.

We found several differences in the profile of macrophage cytokines (normalized to the number of cells-1.5×10^6 in a well) after various modes of cardiac injury (Supplementary Information Fig. S1, Fig. 1c–g). First, we found that neonatal cardiac macrophages secreted relatively high amounts of IL-6, a pleiotropic cytokine involved in inflammation and regeneration after injury, particularly after MI, compared to sham-operated neonatal hearts (Fig. 1c). Second, myocardial injury triggered cardiac macrophages to secrete significant amounts of OPN, a pleiotropic matricellular protein (Fig. 1d). Macrophage secretion of IL-10 (Fig. 1e), an anti-inflammatory, anti- and pro-fibrotic cytokine, and IL-13 (Fig. 1f), an anti-inflammatory, regenerative cytokine [62], was reduced after cardiac injury, compared with sham operation in neonatal hearts. Surprisingly, neonatal macrophages secreted low amounts of VEGF-A after AR, MI, and sham operation, compared with adult macrophages after MI (Fig. 1g). The latter finding suggests that VEGF-A does not mediate the regenerative properties of neonatal macrophages. Given the cytokine array findings, we aimed to determine the role of OPN in myocardial regeneration.

Impaired myocardial healing in OPN-deficient Mice

To determine the effect of OPN deficiency on myocardial regeneration and repair in neonatal hearts, we used 150 C57BL/6 OPN-deficient mice and 51 C57BL/6 (wild-type control) mice. Postoperative survival immediately after surgery was similar in the OPN deficient vs. control mice: 71 of 150 (47%) and 22 of 51 (43%). Survival on day 1 after surgery was similar in the OPN deficient vs. control mice: 20 of 150 (13%) vs. 8 of 51 (15%) on day 1. However, subsequent survival was lower in OPN $^{-/-}$ mice than in control: day 2 survival was 7 of 150 (4.6%) vs. 5 of 51 (10%) ($p=0.18$), and 3-day survival was 4 of 150 (2.6%) vs. 5 of 51 (10%) ($p=0.047$). Finally, among animals that

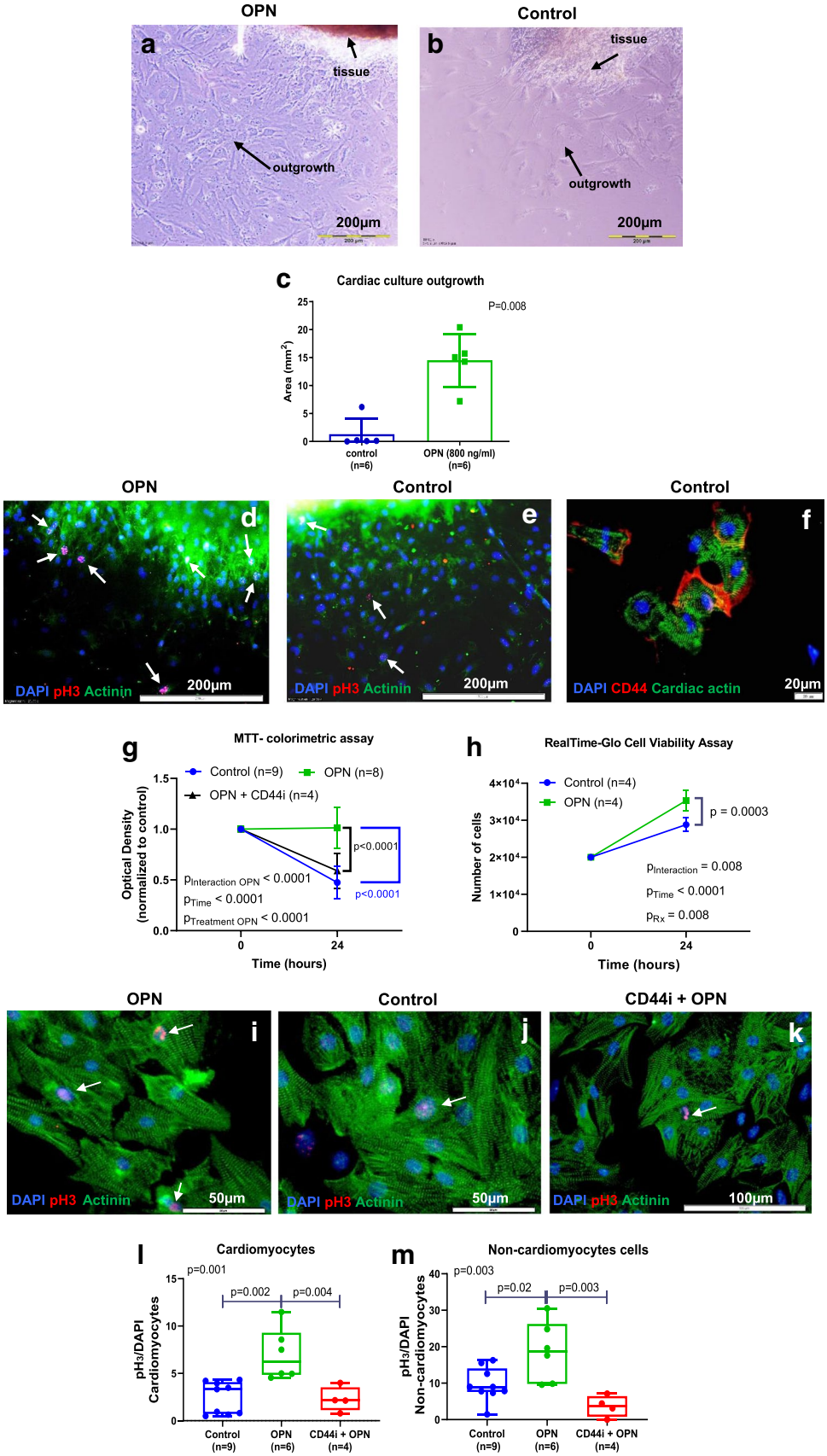
OPN
Control
a
tissue
outgrowth
200µm
b
tissue
outgrowth
200µm
c
Cardiac culture outgrowth
P=0.008
Area (mm²)
control (n=6)
OPN (800 ng/ml) (n=6)
OPN
Control
Control
d
DAPI pH3 Actinin
200µm
e
DAPI pH3 Actinin
200µm
f
DAPI CD44 Cardiac actin
20µm
g
MTT- colorimetric assay
Control (n=9)
OPN (n=8)
OPN + CD44i (n=4)
Optical Density (normalized to control)
p<0.0001
p<0.0001
pInteraction OPN < 0.0001
pTime < 0.0001
pTreatment OPN < 0.0001
Time (hours)
h
RealTime-Glo Cell Viability Assay
Control (n=4)
OPN (n=4)
p = 0.0003
Number of cells
pInteraction = 0.008
pTime < 0.0001
pRx = 0.008
Time (hours)
OPN
Control
CD44i + OPN
i
DAPI pH3 Actinin
50µm
j
DAPI pH3 Actinin
50µm
k
DAPI pH3 Actinin
100µm
l
Cardiomyocytes
p=0.001
p=0.002
p=0.004
pH3/DAPI Cardiomyocytes
Control (n=9)
OPN (n=6)
CD44i + OPN (n=4)
m
Non-cardiomyocytes cells
p=0.003
p=0.02
p=0.003
pH3/DAPI Non-cardiomyocytes
Control (n=9)
OPN (n=6)
CD44i + OPN (n=4)

◂**Fig. 2** OPN stimulated cardiac cell growth. **a**, **b** To determine the effect of OPN on the expansion of cardiac cells, we used a model of cardiac organ culture. Cardiac explants were derived from the heart of a 1-day-old ICR mouse. The explants were treated with OPN (800 ng/ml) or a control medium for 72 h, and the area of cell outgrowth was photographed and measured. We used a single field of × 100 magnification for each well, 5 wells for each treatment. **c** The outgrowth of cells was greater by > 11-fold after treatment with 800 ng/ml OPN compared with control media. **d**, **e** The outgrowth of cardiac cells was immune-stained for the nuclear marker of mitotic activity pH3 (red), cardiac actinin (green), and DAPI (blue) for nuclei. Representative images show that OPN increased the number of pH3-positive cells (**d**) compared with control (**e**). (Images obtained with a single field of × 100 magnification.) **f** Staining for the OPN receptor CD44 (red) and CM actinin (green) revealed positive CD44 expression on nCMs. **g** To determine the effect of OPN on the expansion of cultured CMs, we grew neonatal mouse CMs in a low glucose medium and treated them with (800 ng/ml) or without OPN or anti-CD44 antibody for 24 h. The colorimetric assay MTT determined the number of cells. After 24 h, the CM amount was preserved by OPN. On the other hand, the amount of CMs was decreased without OPN or after adding a CD44 blocker. **h** To confirm the effect of OPN on CM expansion, we used the RealTime-Glo™ MT Cell Viability Assay with (800 ng/ml) or without OPN in a low-glucose medium for 24 h. By this assay, OPN treatment increased the number of cells compared with control. The number of cells was calculated by using the average OD value of 2×10^4 cells at time 0 h: (24 h OD value/ average 0 h OD value) × 2×10^4 cells = the number of cells. **i**–**m** To determine the effect of OPN on the mitotic activity in nCMs, we extracted and cultured nCMs from 1-day-old C57BL/6 mice. The purity of nCMs was 85% after 24 h in culture. The cultured cells were treated with 800 ng/ml OPN (**i**), without OPN (**j**) or a combination of 10 µg/ml CD44i and 800 ng/ml OPN (**k**) for 24 h and then stained for pH3 (red), actinin (green), and DAPI (blue) for nuclei. The percentage of mitotic activity in nCMs was indicated by nuclear pH3 positive nCMs (arrows). The percentage of pH3 nCMs was calculated based on 4 different experiments, 3 wells for each treatment group, in 4 fields of × 100 magnification per well. **l** The percentage of pH3 positive nCMs was higher after OPN therapy compared with the control and the combination of OPN and CD44i groups. **m** To determine the effect of OPN on mitotic activity in non-nCMs, we counted non-nCM cells that expressed pH3. Cells that did not stain for Actinin were considered as non-nCMs. The cultured cells were treated with 800 ng/ml OPN, without OPN or with a combination of 10 µg/ml CD44i and 800 ng/ml OPN for 24 h and then stained for pH3. Compared with the control and the combination groups, the percentage of pH3-positive non-nCM cells was higher after OPN therapy. Differences between groups were tested by nonparametric Mann–Whitney test or Kruskal–Wallis test (> 2 groups), followed by Dunn's multiple comparisons post-test. To assess differences in nCM activity by colorimetric assay, over time, with and without OPN therapy, we used two-way repeated-measures ANOVA. We used Holm-Šídák's multiple comparisons post-test to assess the significance of predefined comparisons at specific time points. *CD44i* CD44 inhibitor, *H&E* hematoxylin and eosin, *DAPI* 4′,6-diamidino-2-phenylindole, *MSC* mesenchymal stromal cell, *MTT* 3-(4,5-dimethylthiazol-2-yl)-2,5-diphenyltetrazolium bromide, *nCMs* neonatal cardiomyocytes, *OD* optical density, *OPN* osteopontin, $OPN^{-/-}$ osteopontin knockout, *pH3* phosphohistone-H3, *PI* propidium iodide, *WT* wild-type

survived the AR operation, the 3-day survival was significantly lower in OPN-deficient mice than in control mice: 4 of 71 (5.6%) vs. 5 of 22 (22.7%); ($p = 0.03$). These favorable effects on survival suggest that OPN is essential for myocardial healing, regeneration, and repair.

Histologic examination revealed that $OPN^{-/-}$ hearts developed loose granulation tissue with large cavities at the injured site and incomplete healing of the myocardium on day 3 after AR (Fig. 1h, i). The impaired healing in OPN KO hearts contradicted the healing process and compact granulation tissue formation that characterized AR in neonatal control hearts (Fig. 1j, k) [22, 42]. Moreover, the areas of inflammation and granulation tissue formation were significantly greater in OPN deficient hearts than in WT control, 3 days after AR (Fig. 1l). Together, our findings suggest that OPN is essential for healing in the neonatal heart.

OPN stimulated the growth of neonatal heart tissue

To further investigate the effects of OPN on myocardial tissues, we used the organ culture technique [8, 22]. First, we harvested one-day-old mouse hearts ($n = 18$), sectioned them into 0.5–1 mm pieces, and then cultured the explants. Next, the explants were treated with 800 ng/ml of OPN or a culture medium as a control. The dose of OPN was determined based on preliminary toxicity studies and previous reports [1, 9, 56].

After 72 h, we observed the outgrowth of cardiac cells from the cultured heart tissues (Fig. 2a, b). The outgrowth area was more than 11 times greater after OPN treatment than the medium treatment (Fig. 2c). Staining of cardiac tissues for phosphohistone-3 (pH3), a marker of mitotic activity, revealed a higher expression of pH3 after treatment with 800 ng/ml of OPN (Fig. 2d), compared with those in non-treated tissues (Fig. 2e). Most of the pH3-positive cells were non-CM cells. Together, our results indicate that OPN stimulates cardiac cell mitotic activity and growth.

OPN promoted cell-cycle activity in nCMs via CD44

The proliferation of resident CMs underlies myocardial regeneration in the neonatal heart [2, 42]. To determine whether OPN can specifically stimulate CM proliferation, first, we stained nCMs for CD44, the OPN receptor. CD44 mediates some OPN mitotic effects [19]. nCM purity was 85% after 24 h. CD44 staining showed that wild-type and OPN-deficient nCMs express membranous CD44 (Fig. 2f and Supplementary Fig. S2).

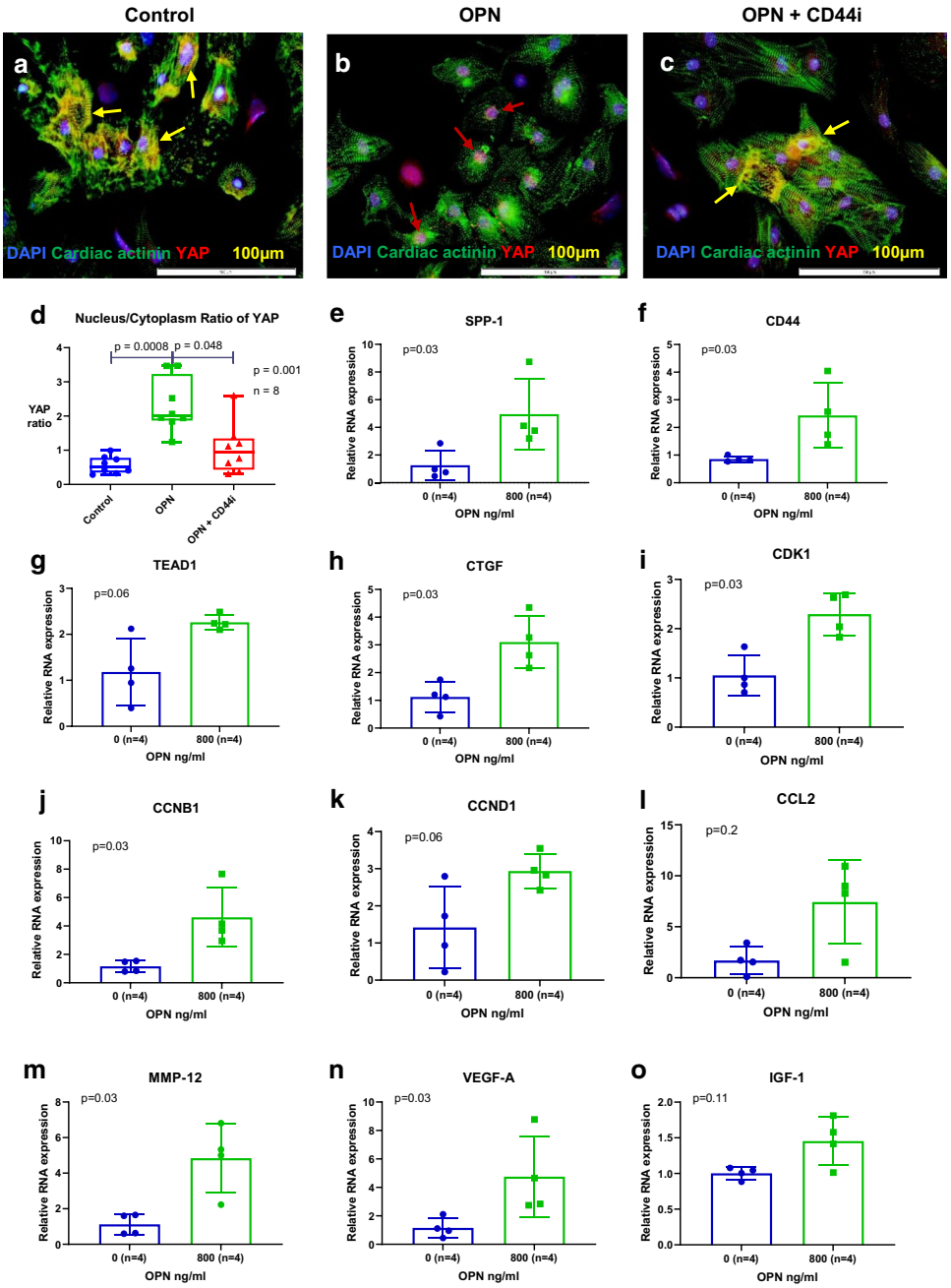

To determine the effect of OPN on nCM number and viability, we used 2 assays. First, we used a 3-(4,5-dimethylthiazol-2-yl)-2,5-diphenyltetrazolium bromide (MTT) colorimetric assay to assess nCM viability and number under stress (low-glucose medium and without serum). While the number of untreated cells decreased, OPN treatment preserved the number of nCMs in a low-glucose medium for 24 h (Fig. 2g). Significantly, CD44 antibodies that block the OPN receptor CD44 (CD44i) abolished the favorable effect of OPN on nCM number (Fig. 2g).

To further confirm the favorable effect of OPN on cultured nCM viability and number, we used another cell viability assay: RealTime-Glo™. Bioluminescent analysis indicated that OPN increased the number of nCMs compared

◂**Fig. 3** OPN stimulated the cell cycle in nCMs. To explore the downstream signaling pathways underlying the effects of OPN, we grew nCMs in a low-glucose medium and treated them with 800 ng/ml of OPN, or 800 ng/ml of OPN plus CD44 blocker. The cells were stained with DAPI (blue) for nuclei, cardiac actinin (green) for CMs, and YAP (red). **a** Microscopic examination of the untreated cells revealed that YAP (red) is localized to the cytoplasm (arrows). **b** Adding OPN to the medium shifted YAP (red) from the cytoplasm into the nucleus (arrows). **c** Adding a CD44 blocker abolished the shift of YAP into the nucleus (arrows). **d** To measure the extent of nuclear translocation of YAP, we quantified the ratio of nuclear to cytoplasmatic YAP fluorescent intensity. First, we obtained microscopic images of each well, 2 wells per treatment group, 4 images per well. Then, using a macro-based algorithm in ImageJ 1.52p, we measured the fluorescent intensity within specific areas and calculated the ratio of nuclear to cytoplasmatic YAP staining (red for YAP, blue for DAPI, and green for cytoplasmatic actin). Quantifying YAP staining showed that OPN increased YAP nuclear localization by fourfold compared with control. By adding a CD44 blocker, we abolished the nuclear translocation of YAP. Together, our data indicate that activation of CD44 by OPN induces nuclear translocation of YAP in nCMs. Statistical analysis was done by the Kruskal–Wallis test and Dunn's multiple comparisons post-test. **e**–**o** Gene expression analysis, using qRT-PCR, was performed in nCMs treated with or without 800 ng/ml OPN for 24 h. qRT-PCR $2^{-\Delta\Delta CT}$ was calculated using GAPDH as an endogenous control. qRT-PCR revealed that OPN upregulated the expression of the OPN gene SPP-1 (**e**) and its receptor CD44 (**f**), as well as cell-cycle genes, including the transcriptional enhancer factor TEF-1 (TEAD1) (**g**), connective tissue growth factor (CTGF) (**h**) and the YAP downstream target cyclin-dependent kinase 1 (CDK1) (**i**). Furthermore, OPN upregulated cyclin B1, a regulator of the mitotic phase (**j**), and CCND1, (**k**) that encodes cyclin D1. OPN also upregulated several reparative genes in nCMs, including the monocyte chemokine CCL2 (chemoattractant protein 1) (**l**), MMP-12 (**m**), VEGF-A (**n**), and insulin-like growth factor -1 (IGF-1) (**o**). Statistical analysis was performed using the nonparametric Mann–Whitney test. *CCNB1* cyclin B1, *CCND1* cyclin D1, *CCL2* chemokine (C–C motif) ligand 2, *CDK1* cyclin-dependent kinase 1, *CTGF* connective tissue growth factor, *ERK* extracellular signal-regulated kinases, *kDA* kilodalton, *IGF-1* insulin-like growth factor-1, *MMP-12* matrix metallopeptidase 12, *nCMs* neonatal cardiomyocytes, *OPN* osteopontin, *pERK* phosphor extracellular signal-regulated kinases, *pLATS* phospho Large tumor suppressor kinase, *pMST1* phospho macrophage-stimulating 1, *pYAP* phospho yes-associated protein, *SPP-1* secreted phosphoprotein 1, *TEAD1* transcriptional enhancer factor TEF-1, *VEGF* vascular endothelial growth factor

with untreated cells (Fig. 2h). Overall, our data indicate that OPN expands the number of nCMs under stress, and CD44 mediates these favorable effects.

To investigate the effect of OPN on nCMs mitotic activity, we treated nCMs with 800 ng/ml of OPN with or without CD44i. We found that OPN increased the expression of pH3, a marker of mitotic activity, in nCMs by 2.8-fold and in non-nCM by 1.9-fold, compared with control cells (Fig. 2i–m). To determine whether blocking the OPN receptor CD44 would decrease cell cycle activity, we exposed neonatal cardiac cells to OPN with and without CD44. Blocking CD44 abolished the OPN-induced upregulation of pH3 in both nCMs and non-nCMs) cardiac actin negative) cells (Fig. 2k–m). Together, these results supported the results from viability assays and indicated that CD44 mediates the effect of OPN on cell cycle activity and viability.

OPN increased nuclear localization of yes-associated protein 1 (YAP1)

The Hippo signaling pathway is an evolutionarily ancient cascade of kinases and proteins that control cell proliferation and organ size [67]. Inactivating the Hippo pathway, or activation of its downstream effector, the YAP transcription co-activator, stimulates myocardial regeneration [64, 68]. YAP is transcriptionally active when it is localized to the nucleus. To determine whether YAP mediates the downstream signaling underlying the actions of OPN, we performed YAP-1 immunostaining. While in untreated nCMs, YAP was mainly localized to the cytoplasm (Fig. 3a), treatment with OPN translocated YAP to the nuclei (Fig. 3b). Notably, the blockage of CD44 eliminated the OPN-induced YAP translocation (Fig. 3c). To estimate the magnitude of nuclear translocation of YAP, we calculated the ratio of nuclei to cytoplasm YAP. Quantification of YAP fluorescent intensity showed that OPN treatment increased nuclear localization of YAP by fourfold, compared with no treatment. Notably, the CD44 blocker diminished the nuclear translocation of YAP (Fig. 3d). Together, our data indicate that activating CD44 by OPN signals nuclear translocation of YAP in nCMs.

OPN upregulated cell-cycle genes

To deeper investigate the effects of OPN on the cell cycle, we analyzed gene expression in nCMs with and without OPN treatment. Gene expression analysis revealed that OPN upregulated the expression of genes such as the OPN gene SPP-1 (Fig. 3e) and its receptor CD44 (Fig. 3f). In addition, OPN also upregulated the expression of the transcriptional enhancer factor TEF-1 (TEAD1) (Fig. 3g) that interacts with YAP1 as well as YAP downstream target genes such as connective tissue growth factor (CTGF) (Fig. 3h) and cyclin-dependent kinase 1 (CDK1) (Fig. 3i). Furthermore, OPN upregulated CCNB1 that encodes cyclin B1 (Fig. 3j), a regulator of the mitotic (M) phase, and CCND1 (Fig. 3k) that

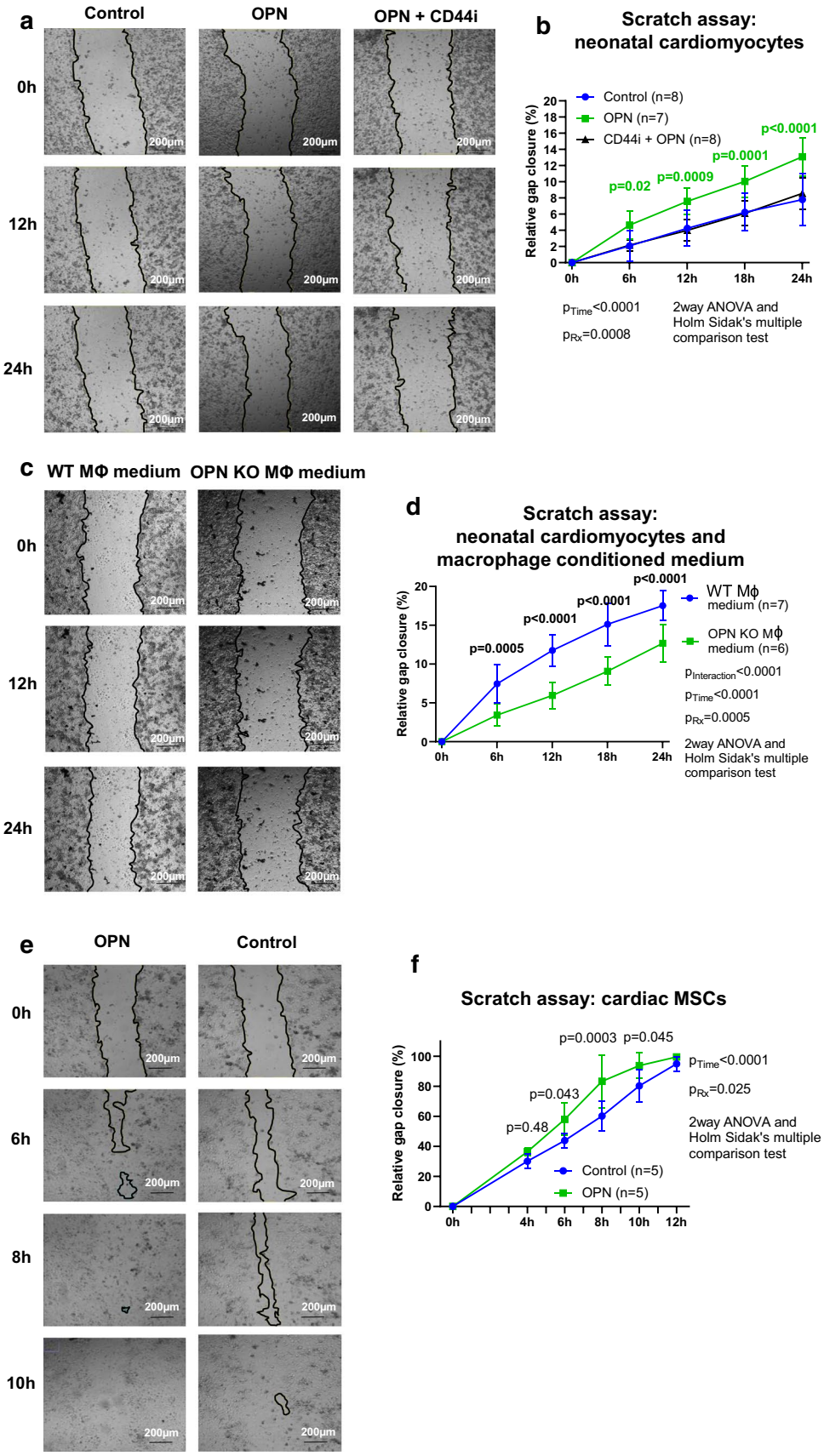

Fig. 4 OPN stimulated proliferation and migration of cardiac cells. To determine the effects of OPN on the migration of cardiac cells, we used the wound healing scratch assay. **a**, **b** First, we used a scratch assay in cultured nCMs of a newborn mouse. We scratched the sheet of nCMs with the tip of a 10 µl pipette. Next, we exposed the nCMs to a low-glucose medium with or without 800 ng/ml of OPN, or 800 ng/ml of OPN with a CD44 blocker, for 24 h. **a** Representative images of gap closure of nCMs. **b** OPN accelerated the rate of gap closure ([(Area of the gap at t_0 − Area of the gap at t_x)/ Area of the gap at t_0]×100) in CMs. Adding a CD44 blocker eliminated the favorable effects of OPN on CMs. To confirm the regenerative properties of macrophage OPN, we collected conditioned medium from cultured macrophages isolated from wild-type or OPN deficient adult female mice 3 days after MI. **c** Representative images of gap closure of nCMs. **d** Conditioned medium from WT cardiac macrophages accelerated gap closure in nCMs to a higher degree than conditioned medium from OPN deficient macrophages. These findings indicate impaired reparative paracrine properties of OPN deficient macrophages. To determine the effect of OPN on cardiac MSCs migration and proliferation, we used the wound healing scratch assay in cultured MSCs of newborn C57BL/6 mice. Neonatal cardiac MSCs were treated with or without 800 ng/ml OPN for 12 h. **e** Representative images of gap closure in OPN-treated and untreated MSCs. **f** OPN accelerated the rate of gap closure compared with control. P values were calculated by the Mann–Whitney test or repeated measures two-way ANOVA and Holm-Šídák's multiple comparisons post-test. *CD44i* CD44 inhibitor, *MSCs* mesenchymal stromal cells, *nCMs* neonatal cardiomyocytes, *OPN* osteopontin, *WT* wild-type

encodes cyclin D1. The latter cell-cycle genes are associated with CM proliferation [32]. Thus, overall, OPN upregulated cell-cycle genes.

OPN also upregulated other genes that are relevant to myocardial rejuvenation. These genes included the chemokine CCL2 (Fig. 3l), matrix metallopeptidase (MMP)-12 (Fig. 3m), VEGF-A (Fig. 3n), and insulin-like growth factor-1 (IGF-1) (Fig. 3o), which encodes the trophic factor IGF-1. Upregulation of these genes can contribute to heart rejuvenation.

In summary, our data indicate that OPN stimulates cell-cycle activity and expression of reparative genes in nCMs via the CD44 receptor and nuclear translocation of YAP-1. Given that macrophages are a primary source of OPN after myocardial injury [33], our results suggest another mechanism by which macrophages contribute to neonatal heart regeneration.

OPN facilitated propagation and migration of nCMs

To determine the effect of OPN on the reparative properties of nCMs, we simulated myocardial regeneration in vitro. We exposed cultured beating nCMs to a "wound healing" scratch assay and subsequent OPN (800 ng/ml) or culture medium treatment. After 24 h, OPN treatment accelerated the rate of gap closure of beating nCMs compared with untreated beating nCMs (Fig. 4a, b, Supplementary Information Video 1). Blocking CD44 by adding CD44 antibodies to the culture medium eliminated the favorable effect of OPN (Fig. 4b). The latter result indicated that CD44 mediates the effects of OPN on the proliferation and migration of nCMs. Overall, OPN stimulates nCM propagation and migration, critical elements of myocardial regeneration [20].

Finally, we used the nCMs scratch assay to assess the regenerative properties of macrophage OPN. We isolated cardiac macrophages from wild-type and OPN-deficient adult female mice three days after MI. Macrophages were cultured for 24 h, and the conditioned medium was collected and analyzed. The protein concentration in the WT and OPN KO macrophage media was 28.5 µg/ml and 28.8 µg/ml. However, while the concentration of OPN in the conditioned medium from the WT macrophages was 102.94 pg/mL, the OPN concentration from the OPN KO macrophage medium was below the threshold of detection. Notably, conditioned medium from OPN-deficient macrophages was less effective than conditioned medium from WT cardiac macrophages in stimulating proliferation and migration of nCMs (Fig. 4c, d). These findings indicate impaired reparative properties of OPN deficient macrophages.

OPN facilitated proliferation and migration of MSCs and ECs

MSCs exert immunoregulatory and reparative functions and provide paracrine and structural support to tissue regeneration and repair [21]. To investigate the effect of OPN on cardiac MSCs, we repeated the scratch assay with neonatal cardiac MSCs (Fig. 4e). Gap closure in cardiac MSCs was 30 times faster than in CMs, with complete closure of the gap within 12 h, with and without OPN (Fig. 4e, f). Our results confirm that MSCs and fibroblasts have much higher turnover rates than CMs [7]. Still, OPN accelerated the rate of gap closure in neonatal cardiac MSCs, compared with no treatment (Fig. 4f). Together, our functional in vitro studies indicate that OPN stimulates the proliferation and migration of both nCMs and MSCs.

Angiogenesis is an essential factor in myocardial regeneration and repair [2]. To determine the effect of OPN on angiogenesis, we used the angiogenic tube formation assay (Supplementary Information Fig. S3). Incremental doses of OPN stimulated the generation of EC tubes, as assessed by the number of polygons (Supplementary Information Fig. S3a, b). Overall, our findings confirmed and expanded upon previous reports regarding the ability of OPN to stimulate angiogenesis [10].

OPN improved LV remodelling and function after MI in adult mice

To examine the relevance of our results in vitro to infarct repair, we allocated 12-week-old C57BL/6 female mice to MI ($n=82$), with a single injection of OPN (200 ng) ($n=20$) or saline ($n=19$) into the ischemic zone after coronary artery occlusion. Post MI mortality was 34% (28 of 82). Animals with small or no MI indicated by LVEF > 40% on day 1 after MI were excluded from the analysis (7 from the OPN group and 8 from the control group). Thus, the final analysis included 39 mice (20 treated by OPN and 19 control).

We assessed LV remodelling and global and regional function by echocardiography and speckle-tracking-based strain imaging (Fig. 5 and Supplementary Information Tables S2, S3, and S4). Compared with control, OPN therapy prevented diastolic thinning and improved systolic thickening of the LV anterior wall (infarct-related segments) and remote posterior LV segments (Fig. 5a–d), reduced LV dilatation (Fig. 5e–j), and improved LV contractility (Fig. 5k–m), 30 days after MI. In addition, the increased thickness of remote LV segments, such as the posterior LV wall, is compatible with the trophic effects of OPN [16].

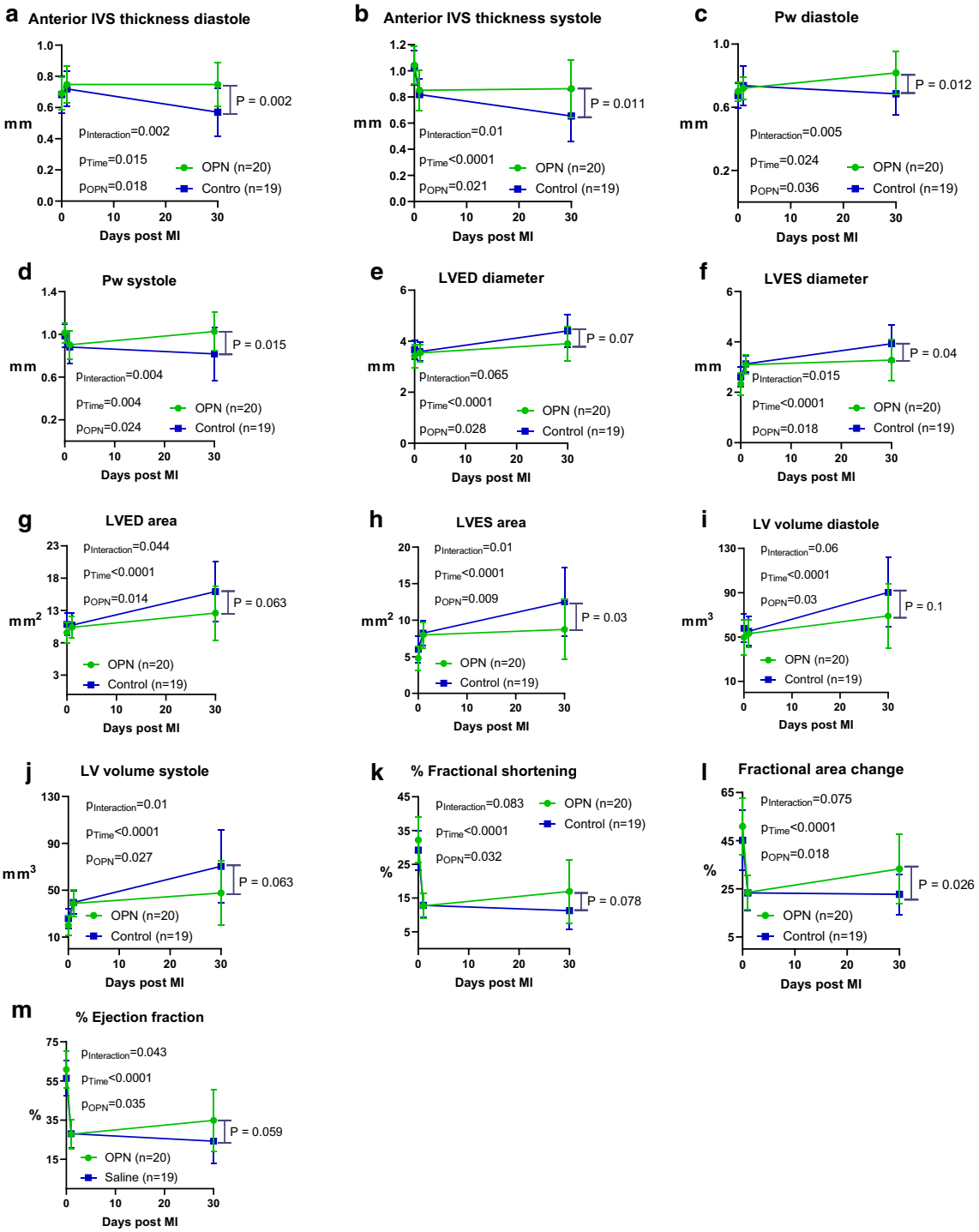

Fig. 5 OPN improved LV remodelling and function after MI. To determine the effects of OPN on adult hearts, we allocated 12-week-old C57BL/6 female mice to MI and a single intra-myocardial injection of OPN (200 ng) or saline. LV remodelling, global, and regional function were assessed by echocardiography before, 1, and 30 days after MI. **a**, **b** OPN prevented diastolic thinning (**a**) and improved systolic thickening (**b**) of the anteroseptal wall (infarct-related LV segments). **c**, **d** OPN improved diastolic and systolic thickening of the posterior wall. **e**–**j** OPN reduced diastolic and systolic LV dilatation as indicated by reduced LVEDD (**e**), LVESD (**f**), LVED area (**g**), LVES area (**h**), diastolic LV volume (**i**), and LV systolic volume (**j**). **k**–**m** OPN improved LV contractility as indicated by improved fractional shortening (FS) (**k**), endocardial fractional area change (FAC) (**l**), and LV ejection fraction (LVEF) (**m**), 30 days after MI. Statistical analysis was performed using repeated measures two-way ANOVA and Holm-Šídák's multiple comparisons post-test. *AW* anterior wall, *Dia* diastolic, *EF* ejection fraction, *FAC* fractional area change, *FS* fractional shortening, *LV* left ventricular, *LVED* left ventricular end-diastolic, *LVEDD* left ventricular end-diastolic diameter, *LVEF* left ventricular ejection fraction, *LVES* left ventricular end-systolic, *LVESD* left ventricular end-systolic diameter, *OPN* osteopontin, *PW* posterior wall, *Sys* systolic

The favorable effects of OPN on myocardial function after MI were partially supported by LV speckle-tracking-based radial strain analysis in short- and long-axis views (Fig. 6 and Supplementary Information Table S3). OPN improved the regional radial strain of the infarcted segments in the long-axis view (Fig. 6a–h). Notably, OPN enhanced the recovery of the apical segments (Fig. 6b, e) prone to dyskinesis and aneurysm formation. In the short-axis view (Fig. 6j–p), OPN improved the recovery of the inferior and posterior segments (Fig. 6l, m). In several segments, the favorable effects appeared early, within 1 day after MI (Fig. 6m, n, p). Overall, OPN therapy improved the recovery of specific segments after MI.

OPN promoted CM mitotic activity and improved infarct repair

Assessment of infarct morphology and histology provided further insight into the mechanism by which OPN improved cardiac function. Mice were subjected to MI and treated with a single injection of recombinant OPN (200 ng) or saline to the border of the ischemic zone after coronary artery ligation.

First, we examined whether OPN could induce CM cell-cycle activity in vivo. We assessed cell-cycle re-entry by the percentage of pH3-positive CMs in the border zone adjacent to the infarcted tissue 3 days after MI (Fig. 7a, b). OPN treatment increased cell-cycle re-entry in CMs by 3.4-fold compared with control (Fig. 7c). Thus, although a rare event, OPN stimulated cell-cycle re-entry in adult CMs after MI.

Finally, postmortem morphometric analysis (Supplementary Information Table S5) revealed that OPN increased scar thickness and reduced scar length, compared with control (Fig. 7d, e), 30 days after MI. Quantitative analysis revealed that OPN increased the average scar thickness by 2.3-fold, compared with control (Fig. 7f). This is significant because wall stress and the degree of infarct dyskinesis and LV dilatation are reduced by scar thickening (Laplace's law). Compared with control, OPN reduced scar length by fourfold (Fig. 7g) but did not affect the total and relative scar area (Fig. 7h, Supplementary Information Table S5). OPN slightly reduced LV area (Fig. 7i) and LV cavity area (Fig. 7j) but did not affect LV muscle area (Supplementary Information Table S5). Significantly, OPN reduced the LV expansion index by 4.4-fold, compared with control, 30 days after MI (Fig. 7k). In summary, morphometry results supported the echocardiography results and confirmed the favourable effects of OPN on infarct repair, scar formation, and LV remodelling.

Discussion

Our work provides several new findings. First, we show, for the first time, that after injury in the neonatal heart, cardiac macrophages secrete high amounts of OPN, which is essential for myocardial healing. Second, OPN deficiency in neonatal mice impaired healing after myocardial injury. Third, OPN deficiency in cardiac macrophages impairs paracrine reparative properties. Fourth, we show that recombinant OPN triggers cell-cycle re-entry in nCMs by stimulating CD44 and YAP signaling (Fig. 8). Fifth, recombinant OPN affects various cardiac cells other than CMs, including MSCs and ECs. Finally, we translated our results in neonatal hearts into a treatment for acute MI in the adult heart. A single local injection of a high dose of recombinant OPN improved infarct healing and scar formation, reduced LV remodelling, and improved overall cardiac function after MI. Together, our results suggest that OPN is essential for myocardial regeneration and that OPN can be used to stimulate endogenous healing and infarct repair in adult hearts.

OPN in heart repair as a double-edged sword

OPN may play a dual role in the pathogenesis of cardiovascular diseases [29, 53]. OPN is present at low levels under basal conditions [55, 57]. However, OPN is upregulated in acute and chronic injuries [15, 29, 55]. OPN is upregulated in response to MI [33] and is mainly secreted by cardiac reparative macrophages [33, 52]. OPN drives cellular functions that impact cell survival, adhesion, migration, and proliferation [15, 29, 55]. OPN controls macrophage biology and regulates migration, survival, phagocytosis, and cytokine production. In addition, macrophage OPN contributes to the clearance of dead cells essential for tissue healing and reparative scar formation [51, 52].

OPN is also a pro-resolving mediator with anti-inflammatory properties [60]. OPN deficiency resulted in increased LV dilation and worsened cardiac function [57]. In line with the above reports, we show that OPN inspires various cardiac cells (e.g., CMs, MSCs, and ECs) to proliferate, migrate, and improve infarct repair and scar formation. Our results support previous reports on the critical role of OPN in tissue repair [59].

On the other hand, OPN has been linked to the pathogenesis of various myocardial disorders, particularly fibrosis and heart failure. OPN expression coincides with the development of pressure overload-induced heart failure [54, 61] and stimulates a fibrogenic program in cardiac fibroblasts [15]. In aging hearts, adipose tissue OPN promotes cardiac

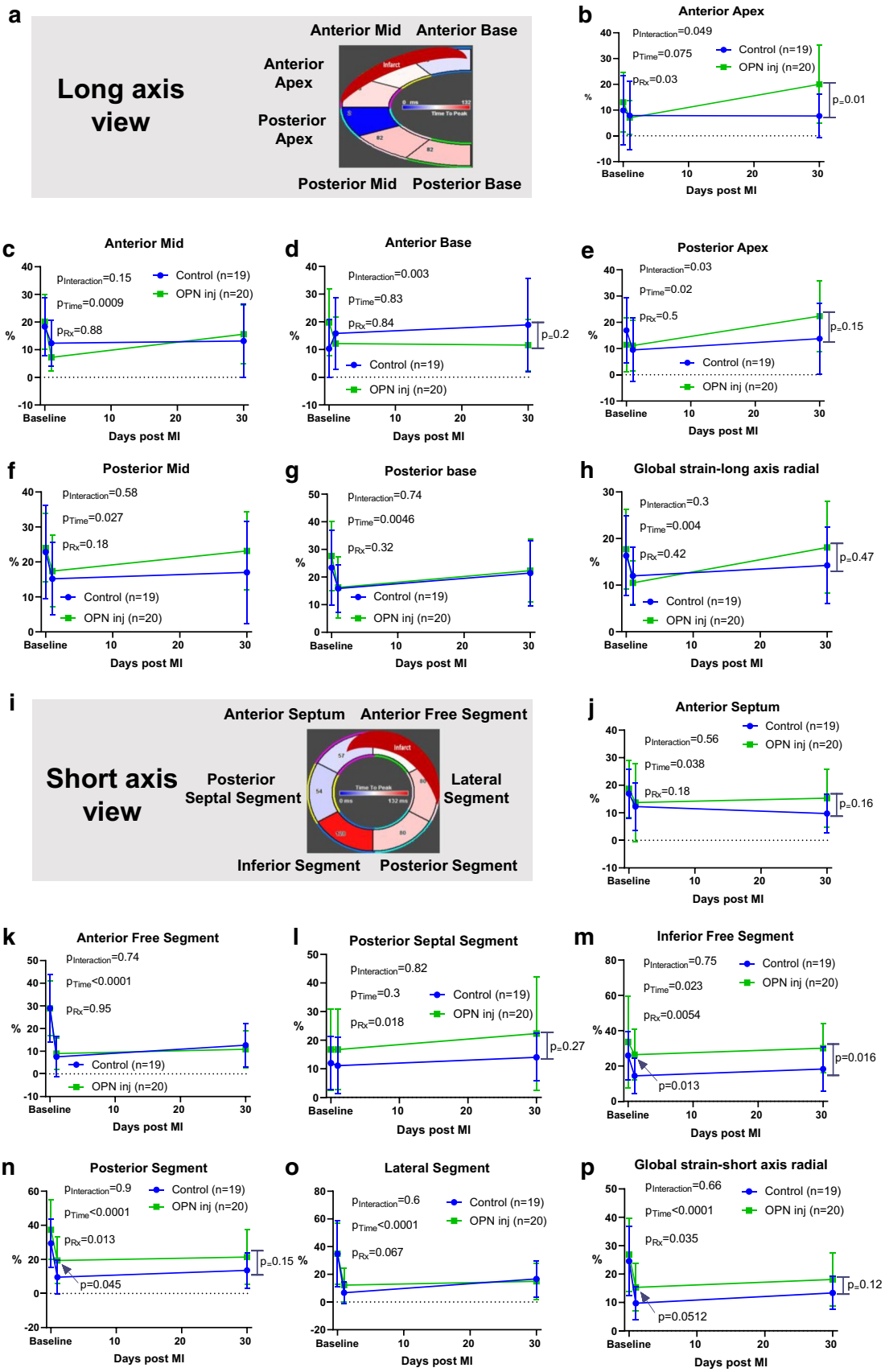
a
Long axis view
Anterior Mid
Anterior Base
Anterior Apex
Posterior Apex
Posterior Mid
Posterior Base
b
Anterior Apex
pInteraction=0.049
pTime=0.075
pRx=0.03
Control (n=19)
OPN inj (n=20)
p=0.01
Baseline
Days post MI
c
Anterior Mid
pInteraction=0.15
pTime=0.0009
pRx=0.88
d
Anterior Base
pInteraction=0.003
pTime=0.83
pRx=0.84
p=0.2
e
Posterior Apex
pInteraction=0.03
pTime=0.02
pRx=0.5
p=0.15
f
Posterior Mid
pInteraction=0.58
pTime=0.027
pRx=0.18
g
Posterior base
pInteraction=0.74
pTime=0.0046
pRx=0.32
h
Global strain-long axis radial
pInteraction=0.3
pTime=0.004
pRx=0.42
p=0.47
i
Short axis view
Anterior Septum
Anterior Free Segment
Posterior Septal Segment
Lateral Segment
Inferior Segment
Posterior Segment
j
Anterior Septum
pInteraction=0.56
pTime=0.038
pRx=0.18
p=0.16
k
Anterior Free Segment
pInteraction=0.74
pTime<0.0001
pRx=0.95
l
Posterior Septal Segment
pInteraction=0.82
pTime=0.3
pRx=0.018
p=0.27
m
Inferior Free Segment
pInteraction=0.75
pTime=0.023
pRx=0.0054
p=0.016
p=0.013
n
Posterior Segment
pInteraction=0.9
pTime<0.0001
pRx=0.013
p=0.15
p=0.045
o
Lateral Segment
pInteraction=0.6
pTime<0.0001
pRx=0.067
p
Global strain-short axis radial
pInteraction=0.66
pTime<0.0001
pRx=0.035
p=0.12
p=0.0512

◂**Fig. 6** OPN improved regional LV function by speckle-tracking-based strain imaging. To confirm the favorable effects of OPN on myocardial function after MI, we used LV speckle-tracking-based radial strain analysis in long (**a**) and short-axis (**i**) views. **a** LV segmentation by the long axis view. **b–g** Radial strain imaging in the long axis view indicated that OPN improved the function of the apical segment (**b**). This segment is prone to dyskinesis and aneurysm formation. The effect of OPN on contractility of other segments: mid-anterior (**c**), anterior base (**d**), posterior apex (**e**), mid-posterior (**f**), and posterior base (**g**), was less significant. **h** OPN mildly improved global radial strain i.e. the average of regional strains across the ventricle, in the long axis view. **i** LV segmentation by the short axis view. **j–o** Radial strain imaging in the short axis view indicated that OPN improved the contractility of the inferior free segment (**m**) but to lesser significance the other segments, including the anterior septum (**j**), anterior free segment (**k**), posterior septal segments (**l**), posterior segment (**n**), and lateral segment (**o**). **p** OPN mildly improved global radial strain, i.e., the average of regional strains across the ventricle, in the short-axis view. Statistical analysis was performed using repeated measures two-way ANOVA and Holm-Šídák's multiple comparisons post-test. *OPN* osteopontin

fibrosis and dysfunction [46]. OPN also has been implicated in the pathogenesis of heart failure with preserved ejection fraction (HFpEF) [65].

Serum OPN has been correlated with skeletal muscle regeneration and proposed as a novel biomarker for muscle regeneration in Duchenne muscular dystrophy in dogs [24]. On the other hand, an age-dependent increase in the levels of OPN inhibits skeletal muscle regeneration in mice [38].

The conflicting findings on the role of OPN in cardiovascular diseases might depend on the pathological process (acute vs. chronic) and the Goldilocks theory [29, 53]. Given the Goldilocks theory, while a robust, sharp, and transient increase in OPN after an acute injury is reparative and protective, a continuous rise in OPN during chronic diseases causes fibrosis and dysfunction. This theory mirrors the concept that while acute inflammation is essential for proper tissue regeneration and repair, prolonged and unresolved inflammation is detrimental and promotes fibrosis and dysfunction [47]. Here, we show that a single local injection of OPN with brief, transient and local effects during infarct healing is therapeutic and avoids the potential risks associated with chronic stimulation of ECM proteins.

CD44 and YAP mediates the effects of OPN on cell-cycle activity

Strategies to promote CM proliferation are an attractive approach to regenerating the myocardium and improving heart function [14, 18, 44, 58]. Several factors and signaling pathways have been identified as modulators of the CM cell cycle [14, 18, 44, 58]. Several studies have reported the ability of various ECM proteins, such as periostin [23] or agrin [3, 4], to stimulate CM proliferation and cardiac regeneration. Despite its broad roles in myocardial biology and pathology [15], the role of OPN in myocardial regeneration remains unclear.

Our data indicate that OPN stimulates CM cell-cycle re-entry by YAP signaling. YAP is the major downstream effector of the Hippo pathway that controls cell growth, tissue homeostasis, and organ size in various organs, including the heart [64, 67]. Here, we show that OPN, via the membranous receptor CD44, promotes nuclear translocation of cytoplasmatic YAP, inducing cell-cycle progression through interaction with TEAD transcription factors. Thus, our results support the putative regulatory role of CD44 in Hippo-YAP signaling [66].

Limitations

Our study has several limitations. First, although we showed that OPN stimulates nCM growth in vitro, we did not prove CM renewal and myocardial regeneration in adult hearts in vivo. Analyzing CM renewal after an injury is complex due to inflammation and proliferation of non-CM cells [14]. Furthermore, markers of proliferation, such as pH3, identify CMs at metaphase or anaphase but cannot discriminate between karyokinesis and cytokinesis [18, 27]. DNA replication does not necessarily result in cell division, as CMs may contain multiple nuclei (polyploidy) during their cell cycle [18, 27]. Other popular markers of CM proliferation, such as Ki67, EdU, and Aurora B-kinase, cannot define CM cytokinesis [27, 63]. Colorimetric assays, such as MTT or RealTime-Glo™ MT Cell Viability Assay, are not CM-specific. Thus, the increase in the colorimetric signal may result from increased proliferation of neonatal MSCs or ECs that are present (in small amounts) in primary nCM cultures. Nevertheless, OPN can improve infarct healing independent of CM renewal: OPN promotes reparative functions in MSCs, ECs, and macrophages (Fig. 8) [52].

Second, we used adhesion and resistance to trypsinization assay to isolate cardiac macrophages. This method yielded a purification efficiency of > 90% based on positive staining for F4/80 [37]. Other methods of tissue macrophage isolation, such as cell sorting or magnetic isolation, may yield a purer macrophage population. However, cell sorting and magnetic isolation may alter macrophage viability and function [31, 39, 41]. In addition, while contamination of

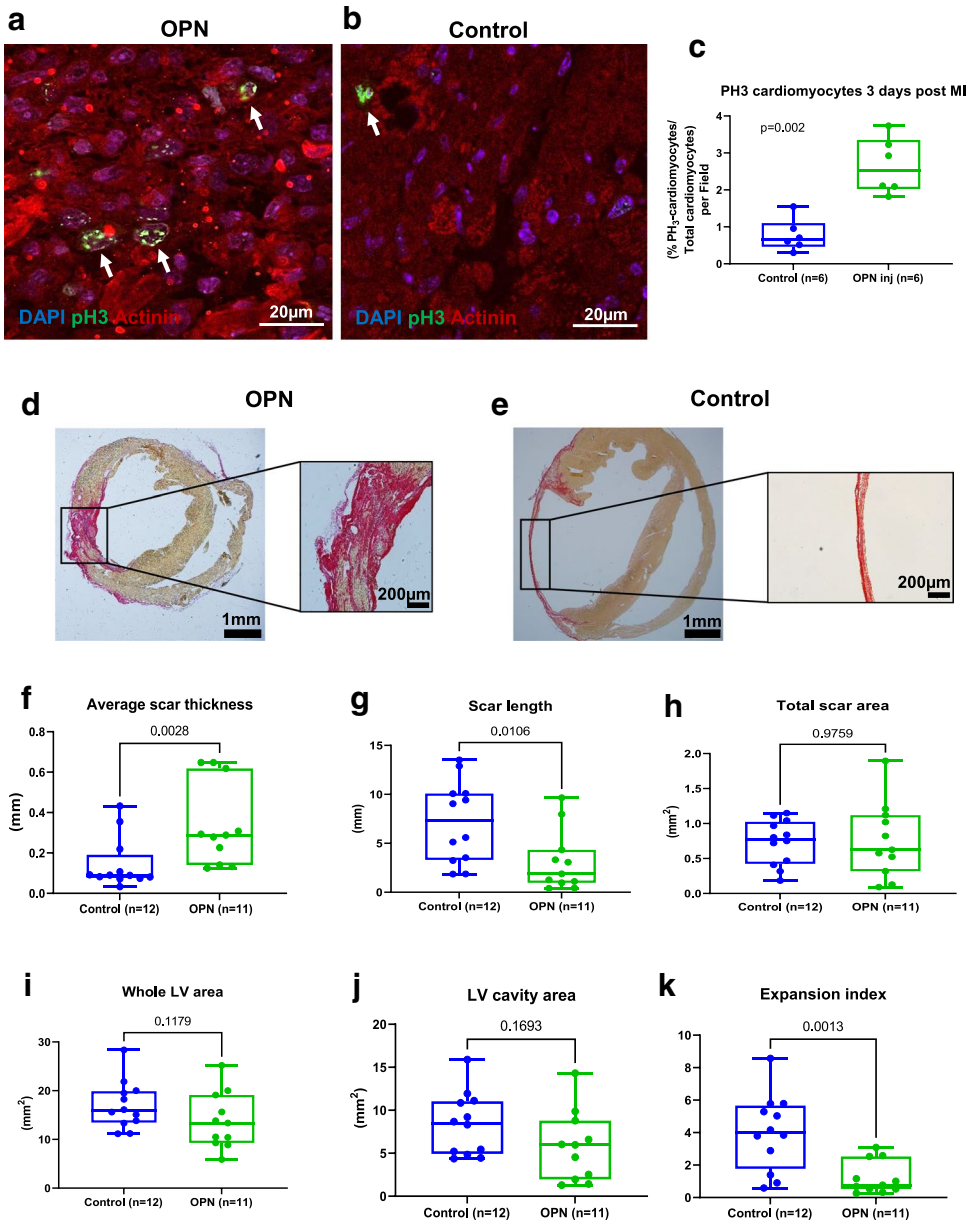

Fig. 7 OPN stimulated CM cell-cycle re-entry and improved scar formation after MI. To determine whether OPN could induce CM cell-cycle activity in vivo, we subjected mice to MI and a single injection of recombinant OPN (200 ng) or saline to the border of the ischemic zone. Three days after MI, the hearts were harvested, sectioned, and slides were stained for pH3 (green), cardiac actinin (red), and DAPI (blue) for nuclei. Microscopic examination of the border zone, 3 days after MI, revealed that OPN increased CM mitotic activity (**a**), indicated by the percentage of pH3-positive CMs (arrows), compared with control (**b**). **c** OPN increased the percentage of pH3-positive CMs by > threefold, at the border zone, compared with control. **d**, **e** Representative images after picrosirius red staining, 30 days after MI, showed that OPN reduced scar length and increased scar thickness (**d**), compared with control (**e**). For postmortem morphometric analysis, we measured LV maximal diameter (defined as the longest diameter perpendicular to a line connecting the insertions of the septum to the ventricular wall), average wall thickness from 3 measurements of septum thickness, average scar thickness from 3 measurements of scar thickness, LV muscle area (including the septum), LV cavity area, whole LV area, epicardial scar length, and endocardial scar length. Relative scar thickness was calculated as average scar thickness divided by average wall thickness. The expansion index was calculated as follows: expansion index = [LV cavity area/whole LV area]/relative scar thickness. **f**–**k** Morphometry analysis revealed that a local OPN injection increased scar thickness (**f**) and reduced the scar length (**g**), compared with control, 30 days after MI. OPN did not affect the scar area (**h**). OPN slightly reduced the LV area (**i**) and the LV cavity area (**j**). OPN reduced the expansion index (**k**), compared with control, 30 days after MI. Statistical analysis was performed using the Mann–Whitney test. *LV* left ventricular, *OPN* osteopontin, *pH3* phosphohistone-H3, *PR* picrosirius red

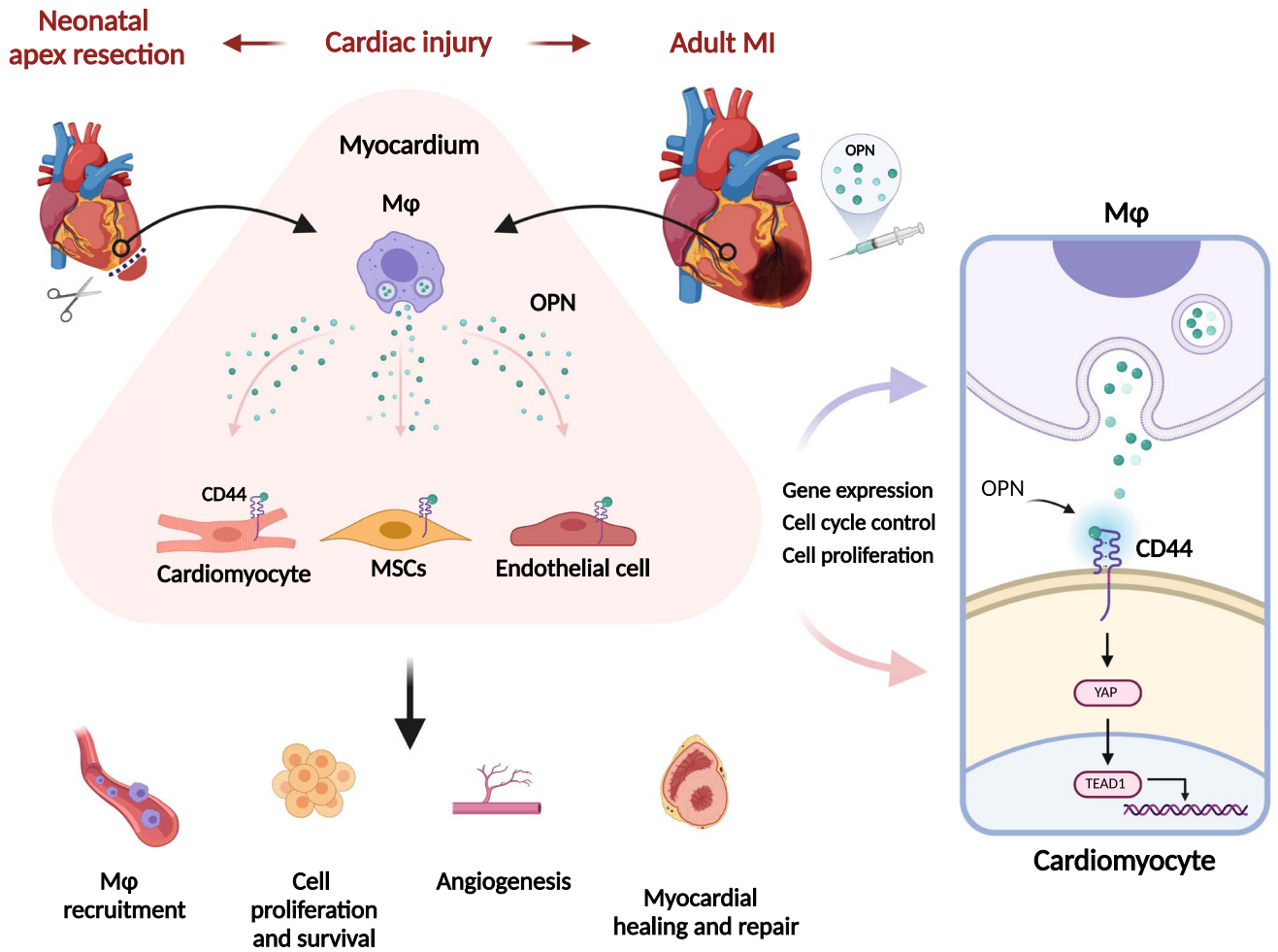

Fig. 8 The proposed pathway by which macrophage OPN improves infarct repair. After a cardiac injury, monocytes and macrophages infiltrate the injured site. Macrophages secrete OPN, affecting multiple cardiac cells such as CMs, MSCs, ECs, and macrophages. Boosting the levels of OPN for a short period stimulates macrophage recruitment, CM cell-cycle re-entry, angiogenesis, and ECM deposition. The mechanism of OPN reparative effects involves CD44-YAP signaling, cardiac cell proliferation, and cell survival. Overall, transient exposure to high levels of OPN improves infarct repair. We created this figure by BioRender.com. *CMs* cardiomyocytes, *EC* endothelial cells, *MSCs* mesenchymal stromal cells, *MΦ* macrophage, *OPN* osteopontin, *TEAD1* transcriptional enhancer factor TEF-1, *YAP* yes-associated protein

macrophage culture with stromal cells may affect the analysis, the residual stromal cells might improve macrophage viability and function [36].

Third, in analysing cytokine release from cardiac macrophages, we did not analyze cytokines from macrophages isolated from sham-operated hearts. Fourth, the timing of OPN administration (one minute after MI) might be clinically limited. Due to the difficulties associated with second thoracotomy and delivery of OPN into the thin (< 0.5 mm) scar of mice after MI, we injected OPN to the border of the ischemic area immediately after MI. Thus, while clinically limited, our results prove that early administration of recombinant OPN improves infarct repair, LV remodelling, and function. Finally, we used an OPN-deficient mouse to isolate the role of OPN in myocardial regeneration. Thus, non-macrophage cells may be affected. Macrophage-specific deletion of OPN might be a better method to confirm the central role of macrophage OPN in myocardial regeneration and repair. Indeed, in vitro experiments with OPN deficient macrophages indicated impaired reparative properties compared with naïve macrophages.

Implications and future research

Our results indicate that OPN is a pleiotropic reparative mediator that activates multiple cardiac cells, stimulates endogenous tissue healing, and improves infarct repair. A better understanding of the role of OPN in myocardial repair and scar formation may promote new therapies to enhance infarct repair.

Supplementary Information The online version contains supplementary material available at https://doi.org/10.1007/s00395-022-00957-0.

Acknowledgements We thank Mrs. Noam Ziv for her skillful English-language editing. We thank Prof. Eldad Tzahor for his critical comments. This work was performed in partial fulfillment of requirements for the Ph.D. degree of Itai Rotem and Tal Konfino, Sackler Faculty of Medicine, Tel Aviv University, Israel.

Author contributions The authors confirm contributions to the paper as follows: study conception and design: IR, TK, and JL; data collection: IR, TK, TC, YS, OS-T, NL, NN-S, DL, DP, and JL; analysis and interpretation of results: IR, TK, TC, YS, OS-T, NL, and JL; draft manuscript preparation: IR, TK, TC, YS, OS-T, NL, NN-S, DL, DP, and JL. All authors reviewed the results and approved the final version of the manuscript.

Funding We gratefully acknowledge support for this project provided by grants from the Seymour Fefer Foundation and the Israel Science Foundation (ISF). Itai Rotem was supported by a Ph.D. scholarship from Mrs. Tuna Gursoy.

Availability of data and material A detailed description of the methods is provided in the Data Supplement Materials. All data that support the findings are available within the article, in the Data Supplement, or upon reasonable request from the corresponding author.

Declarations

Conflict of interest All authors declare that they have no competing interests.

Ethics approval All experimental protocols were approved by the Ethical Committees of the Sheba Medical Center.

References

1. Albertsson AM, Zhang X, Leavenworth J, Bi D, Nair S, Qiao L, Hagberg H, Mallard C, Cantor H, Wang X (2014) The effect of osteopontin and osteopontin-derived peptides on preterm brain injury. J Neuroinflammation 11:197. https://doi.org/10.1186/s12974-014-0197-0
2. Aurora AB, Porrello ER, Tan W, Mahmoud AI, Hill JA, Bassel-Duby R, Sadek HA, Olson EN (2014) Macrophages are required for neonatal heart regeneration. J Clin Invest 124:1382–1392. https://doi.org/10.1172/JCI72181
3. Baehr A, Umansky KB, Bassat E, Jurisch V, Klett K, Bozoglu T, Hornaschewitz N, Solyanik O, Kain D, Ferraro B, Cohen-Rabi R, Krane M, Cyran C, Soehnlein O, Laugwitz KL, Hinkel R, Kupatt C, Tzahor E (2020) Agrin promotes coordinated therapeutic processes leading to improved cardiac repair in pigs. Circulation 142:868–881. https://doi.org/10.1161/CIRCULATIONAHA.119.045116
4. Bassat E, Mutlak YE, Genzelinakh A, Shadrin IY, Baruch Umansky K, Yifa O, Kain D, Rajchman D, Leach J, Riabov Bassat D, Udi Y, Sarig R, Sagi I, Martin JF, Bursac N, Cohen S, Tzahor E (2017) The extracellular matrix protein agrin promotes heart regeneration in mice. Nature 547:179–184. https://doi.org/10.1038/nature22978
5. Bauer M, Cheng S, Jain M, Ngoy S, Theodoropoulos C, Trujillo A, Lin FC, Liao R (2011) Echocardiographic speckle-tracking based strain imaging for rapid cardiovascular phenotyping in mice. Circ Res 108:908–916. https://doi.org/10.1161/CIRCRESAHA.110.239574
6. Ben-Mordechai T, Holbova R, Landa-Rouben N, Harel-Adar T, Feinberg MS, Abd Elrahman I, Blum G, Epstein FH, Silman Z, Cohen S, Leor J (2013) Macrophage subpopulations are essential for infarct repair with and without stem cell therapy. J Am Coll Cardiol 62:1890–1901. https://doi.org/10.1016/j.jacc.2013.07.057
7. Bergmann O, Zdunek S, Felker A, Salehpour M, Alkass K, Bernard S, Sjostrom SL, Szewczykowska M, Jackowska T, Dos Remedios C, Malm T, Andra M, Jashari R, Nyengaard JR, Possnert G, Jovinge S, Druid H, Frisen J (2015) Dynamics of cell generation and turnover in the human heart. Cell 161:1566–1575. https://doi.org/10.1016/j.cell.2015.05.026
8. Blewett CJ, Cilley RE, Ehrlich HP, Blackburn JH 2nd, Dillon PW, Krummel TM (1997) Regenerative healing of incisional wounds in midgestational murine hearts in organ culture. J Thorac Cardiovasc Surg 113:880–885. https://doi.org/10.1016/S0022-5223(97)70260-5
9. Chen W, Ma Q, Suzuki H, Hartman R, Tang J, Zhang JH (2011) Osteopontin reduced hypoxia-ischemia neonatal brain injury by suppression of apoptosis in a rat pup model. Stroke 42:764–769. https://doi.org/10.1161/STROKEAHA.110.599118
10. Dai J, Peng L, Fan K, Wang H, Wei R, Ji G, Cai J, Lu B, Li B, Zhang D, Kang Y, Tan M, Qian W, Guo Y (2009) Osteopontin induces angiogenesis through activation of PI3K/AKT and ERK1/2 in endothelial cells. Oncogene 28:3412–3422. https://doi.org/10.1038/onc.2009.189
11. Deng L, Zhou JF, Sellers RS, Li JF, Nguyen AV, Wang Y, Orlofsky A, Liu Q, Hume DA, Pollard JW, Augenlicht L, Lin EY (2010) A novel mouse model of inflammatory bowel disease links mammalian target of rapamycin-dependent hyperproliferation of colonic epithelium to inflammation-associated tumorigenesis. Am J Pathol 176:952–967. https://doi.org/10.2353/ajpath.2010.090622
12. Ehler E, Moore-Morris T, Lange S (2013) Isolation and culture of neonatal mouse cardiomyocytes. J Vis Exp JoVE 79: e50154. https://doi.org/10.3791/50154
13. Epelman S, Lavine KJ, Beaudin AE, Sojka DK, Carrero JA, Calderon B, Brija T, Gautier EL, Ivanov S, Satpathy AT, Schilling JD, Schwendener R, Sergin I, Razani B, Forsberg EC, Yokoyama WM, Unanue ER, Colonna M, Randolph GJ, Mann DL (2014) Embryonic and adult-derived resident cardiac macrophages are maintained through distinct mechanisms at steady state and during inflammation. Immunity 40:91–104. https://doi.org/10.1016/j.immuni.2013.11.019
14. Eschenhagen T, Bolli R, Braun T, Field LJ, Fleischmann BK, Frisen J, Giacca M, Hare JM, Houser S, Lee RT, Marban E, Martin JF, Molkentin JD, Murry CE, Riley PR, Ruiz-Lozano P, Sadek HA, Sussman MA, Hill JA (2017) Cardiomyocyte regeneration: a consensus statement. Circulation 136:680–686. https://doi.org/10.1161/CIRCULATIONAHA.117.029343
15. Frangogiannis NG (2019) The extracellular matrix in ischemic and nonischemic heart failure. Circ Res 125:117–146. https://doi.org/10.1161/CIRCRESAHA.119.311148
16. Graf K, Do YS, Ashizawa N, Meehan WP, Giachelli CM, Marboe CC, Fleck E, Hsueh WA (1997) Myocardial osteopontin expression is associated with left ventricular hypertrophy. Circulation 96:3063–3071. https://doi.org/10.1161/01.cir.96.9.3063
17. Haubner BJ, Schuetz T, Penninger JM (2016) A reproducible protocol for neonatal ischemic injury and cardiac regeneration in neonatal mice. Basic Res Cardiol 111:64. https://doi.org/10.1007/s00395-016-0580-3
18. He L, Nguyen NB, Ardehali R, Zhou B (2020) Heart regeneration by endogenous stem cells and cardiomyocyte proliferation: controversy, fallacy, and progress. Circulation 142:275–291. https://doi.org/10.1161/CIRCULATIONAHA.119.045566

19. Hsu KH, Tsai HW, Lin PW, Hsu YS, Shan YS, Lu PJ (2010) Clinical implication and mitotic effect of CD44 cleavage in relation to osteopontin/CD44 interaction and dysregulated cell cycle protein in gastrointestinal stromal tumor. Ann Surg Oncol 17:2199–2212. https://doi.org/10.1245/s10434-010-0927-1
20. Itou J, Oishi I, Kawakami H, Glass TJ, Richter J, Johnson A, Lund TC, Kawakami Y (2012) Migration of cardiomyocytes is essential for heart regeneration in zebrafish. Development 139:4133–4142. https://doi.org/10.1242/dev.079756
21. Koliaraki V, Prados A, Armaka M, Kollias G (2020) The mesenchymal context in inflammation, immunity and cancer. Nat Immunol 21:974–982. https://doi.org/10.1038/s41590-020-0741-2
22. Konfino T, Landa N, Ben-Mordechai T, Leor J (2015) The type of injury dictates the mode of repair in neonatal and adult heart. J Am Heart Assoc 4:e001320. https://doi.org/10.1161/JAHA.114.001320
23. Kuhn B, del Monte F, Hajjar RJ, Chang YS, Lebeche D, Arab S, Keating MT (2007) Periostin induces proliferation of differentiated cardiomyocytes and promotes cardiac repair. Nat Med 13:962–969. https://doi.org/10.1038/nm1619
24. Kuraoka M, Kimura E, Nagata T, Okada T, Aoki Y, Tachimori H, Yonemoto N, Imamura M, Si T (2016) Serum osteopontin as a novel biomarker for muscle regeneration in duchenne muscular dystrophy. Am J Pathol 186:1302–1312. https://doi.org/10.1016/j.ajpath.2016.01.002
25. Landa N, Miller L, Feinberg MS, Holbova R, Shachar M, Freeman I, Cohen S, Leor J (2008) Effect of injectable alginate implant on cardiac remodeling and function after recent and old infarcts in rat. Circulation 117:1388–1396. https://doi.org/10.1161/CIRCULATIONAHA.107.727420
26. Lavine KJ, Epelman S, Uchida K, Weber KJ, Nichols CG, Schilling JD, Ornitz DM, Randolph GJ, Mann DL (2014) Distinct macrophage lineages contribute to disparate patterns of cardiac recovery and remodeling in the neonatal and adult heart. Proc Natl Acad Sci U S A 111:16029–16034. https://doi.org/10.1073/pnas.1406508111
27. Leone M, Magadum A, Engel FB (2015) Cardiomyocyte proliferation in cardiac development and regeneration: a guide to methodologies and interpretations. Am J Physiol Heart Circ Physiol 309:H1237-1250. https://doi.org/10.1152/ajpheart.00559.2015
28. Liang CC, Park AY, Guan JL (2007) In vitro scratch assay: a convenient and inexpensive method for analysis of cell migration in vitro. Nat Protoc 2:329–333. https://doi.org/10.1038/nprot.2007.30
29. Lok ZSY, Lyle AN (2019) Osteopontin in vascular disease. Arterioscler Thromb Vasc Biol 39:613–622. https://doi.org/10.1161/ATVBAHA.118.311577
30. Mahmoud AI, Porrello ER, Kimura W, Olson EN, Sadek HA (2014) Surgical models for cardiac regeneration in neonatal mice. Nat Protoc 9:305–311. https://doi.org/10.1038/nprot.2014.021
31. Millard SM, Heng O, Opperman KS, Sehgal A, Irvine KM, Kaur S, Sandrock CJ, Wu AC, Magor GW, Batoon L, Perkins AC, Noll JE, Zannettino ACW, Sester DP, Levesque JP, Hume DA, Raggatt LJ, Summers KM, Pettit AR (2021) Fragmentation of tissue-resident macrophages during isolation confounds analysis of single-cell preparations from mouse hematopoietic tissues. Cell Rep 37:110058. https://doi.org/10.1016/j.celrep.2021.110058
32. Mohamed TMA, Ang YS, Radzinsky E, Zhou P, Huang Y, Elfenbein A, Foley A, Magnitsky S, Srivastava D (2018) Regulation of cell cycle to stimulate adult cardiomyocyte proliferation and cardiac regeneration. Cell 173(104–116):e112. https://doi.org/10.1016/j.cell.2018.02.014
33. Murry CE, Giachelli CM, Schwartz SM, Vracko R (1994) Macrophages express osteopontin during repair of myocardial necrosis. Am J Pathol 145:1450–1462
34. Muzumdar MD, Tasic B, Miyamichi K, Li L, Luo L (2007) A global double-fluorescent Cre reporter mouse. Genesis 45:593–605. https://doi.org/10.1002/dvg.20335
35. Naftali-Shani N, Levin-Kotler LP, Palevski D, Amit U, Kain D, Landa N, Hochhauser E, Leor J (2017) Left ventricular dysfunction switches mesenchymal stromal cells toward an inflammatory phenotype and impairs their reparative properties via toll-like receptor-4. Circulation 135:2271–2287. https://doi.org/10.1161/CIRCULATIONAHA.116.023527
36. Ogawa K, Tsurutani M, Hashimoto A, Soeda M (2019) Simple propagation method for resident macrophages by co-culture and subculture, and their isolation from various organs. BMC Immunol 20:34. https://doi.org/10.1186/s12865-019-0314-z
37. Palevski D, Levin-Kotler LP, Kain D, Naftali-Shani N, Landa N, Ben-Mordechai T, Konfino T, Holbova R, Molotski N, Rosin-Arbesfeld R, Lang RA, Leor J (2017) Loss of macrophage wnt secretion improves remodeling and function after myocardial infarction in mice. J Am Heart Assoc. https://doi.org/10.1161/JAHA.116.004387
38. Paliwal P, Pishesha N, Wijaya D, Conboy IM (2012) Age dependent increase in the levels of osteopontin inhibits skeletal muscle regeneration. Aging (Albany NY) 4:553–566. https://doi.org/10.18632/aging.100477
39. Pfister G, Toor SM, Sasidharan Nair V, Elkord E (2020) An evaluation of sorter induced cell stress (SICS) on peripheral blood mononuclear cells (PBMCs) after different sort conditions—are your sorted cells getting SICS? J Immunol Methods 487:112902. https://doi.org/10.1016/j.jim.2020.112902
40. Phifer CB, Terry LM (1986) Use of hypothermia for general anesthesia in preweanling rodents. Physiol Behav 38:887–890
41. Plouffe BD, Murthy SK, Lewis LH (2015) Fundamentals and application of magnetic particles in cell isolation and enrichment: a review. Rep Prog Phys 78:016601. https://doi.org/10.1088/0034-4885/78/1/016601
42. Porrello ER, Mahmoud AI, Simpson E, Hill JA, Richardson JA, Olson EN, Sadek HA (2011) Transient regenerative potential of the neonatal mouse heart. Science 331:1078–1080. https://doi.org/10.1126/science.1200708
43. Povsic TJ, Sanz-Ruiz R, Climent AM, Bolli R, Taylor DA, Gersh BJ, Menasche P, Perin EC, Pompilio G, Atsma DE, Badimon L, DeMaria AN, Hare JM, Henry TD, Janssens S, Kastrup J, Torella D, Traverse JH, Willerson JT, Fernandez-Aviles F (2021) Reparative cell therapy for the heart: critical internal appraisal of the field in response to recent controversies. ESC Heart Fail. https://doi.org/10.1002/ehf2.13256
44. Sadek H, Olson EN (2020) Toward the goal of human heart regeneration. Cell Stem Cell 26:7–16. https://doi.org/10.1016/j.stem.2019.12.004
45. Sansonetti M, Waleczek FJG, Jung M, Thum T, Perbellini F (2020) Resident cardiac macrophages: crucial modulators of cardiac (patho)physiology. Basic Res Cardiol 115:77. https://doi.org/10.1007/s00395-020-00836-6
46. Sawaki D, Czibik G, Pini M, Ternacle J, Suffee N, Mercedes R, Marcelin G, Surenaud M, Marcos E, Gual P, Clement K, Hue S, Adnot S, Hatem SN, Tsuchimochi I, Yoshimitsu T, Henegar C, Derumeaux G (2018) Visceral adipose tissue drives cardiac aging through modulation of fibroblast senescence by osteopontin production. Circulation 138:809–822. https://doi.org/10.1161/CIRCULATIONAHA.117.031358
47. Sayers JR, Riley PR (2021) Heart regeneration: beyond new muscle and vessels. Cardiovasc Res 117:727–742. https://doi.org/10.1093/cvr/cvaa320
48. Schindelin J, Arganda-Carreras I, Frise E, Kaynig V, Longair M, Pietzsch T, Preibisch S, Rueden C, Saalfeld S, Schmid B, Tinevez JY, White DJ, Hartenstein V, Eliceiri K, Tomancak P, Cardona A

(2012) Fiji: an open-source platform for biological-image analysis. Nat Methods 9:676–682. https://doi.org/10.1038/nmeth.2019
49. Schneider CA, Rasband WS, Eliceiri KW (2012) NIH image to ImageJ: 25 years of image analysis. Nat Methods 9:671–675. https://doi.org/10.1038/nmeth.2089
50. Sharon Y, Raz Y, Cohen N, Ben-Shmuel A, Schwartz H, Geiger T, Erez N (2015) Tumor-derived osteopontin reprograms normal mammary fibroblasts to promote inflammation and tumor growth in breast cancer. Cancer Res 75:963–973. https://doi.org/10.1158/0008-5472.Can-14-1990
51. Shirakawa K, Endo J, Kataoka M, Katsumata Y, Anzai A, Moriyama H, Kitakata H, Hiraide T, Ko S, Goto S, Ichihara G, Fukuda K, Minamino T, Sano M (2020) MerTK expression and ERK activation are essential for the functional maturation of osteopontin-producing reparative macrophages after myocardial infarction. J Am Heart Assoc 9:e017071. https://doi.org/10.1161/JAHA.120.017071
52. Shirakawa K, Endo J, Kataoka M, Katsumata Y, Yoshida N, Yamamoto T, Isobe S, Moriyama H, Goto S, Kitakata H, Hiraide T, Fukuda K, Sano M (2018) IL (Interleukin)-10-STAT3-galectin-3 axis is essential for osteopontin-producing reparative macrophage polarization after myocardial infarction. Circulation 138:2021–2035. https://doi.org/10.1161/CIRCULATIONAHA.118.035047
53. Shirakawa K, Sano M (2021) Osteopontin in cardiovascular diseases. Biomolecules. https://doi.org/10.3390/biom11071047
54. Singh K, Sirokman G, Communal C, Robinson KG, Conrad CH, Brooks WW, Bing OH, Colucci WS (1999) Myocardial osteopontin expression coincides with the development of heart failure. Hypertension 33:663–670
55. Singh M, Foster CR, Dalal S, Singh K (2010) Osteopontin: role in extracellular matrix deposition and myocardial remodeling post-MI. J Mol Cell Cardiol 48:538–543. https://doi.org/10.1016/j.yjmcc.2009.06.015
56. Suzuki H, Ayer R, Sugawara T, Chen W, Sozen T, Hasegawa Y, Kanamaru K, Zhang JH (2010) Protective effects of recombinant osteopontin on early brain injury after subarachnoid hemorrhage in rats. Crit Care Med 38:612–618. https://doi.org/10.1097/CCM.0b013e3181c027ae
57. Trueblood NA, Xie Z, Communal C, Sam F, Ngoy S, Liaw L, Jenkins AW, Wang J, Sawyer DB, Bing OH, Apstein CS, Colucci WS, Singh K (2001) Exaggerated left ventricular dilation and reduced collagen deposition after myocardial infarction in mice lacking osteopontin. Circ Res 88:1080–1087. https://doi.org/10.1161/hh1001.090842
58. Tzahor E, Poss KD (2017) Cardiac regeneration strategies: staying young at heart. Science 356:1035–1039. https://doi.org/10.1126/science.aam5894
59. Wasgewatte Wijesinghe DK, Mackie EJ, Pagel CN (2019) Normal inflammation and regeneration of muscle following injury require osteopontin from both muscle and non-muscle cells. Skelet Muscle 9:6. https://doi.org/10.1186/s13395-019-0190-5
60. Watanabe S, Alexander M, Misharin AV, Budinger GRS (2019) The role of macrophages in the resolution of inflammation. J Clin Invest 129:2619–2628. https://doi.org/10.1172/jci124615
61. Weber A, Büttner AL, Rellecke P, Petrov G, Albert A, Sixt SU, Lichtenberg A, Akhyari P (2020) Osteopontin as novel biomarker for reversibility of pressure overload induced left ventricular hypertrophy. Biomark Med 14:513–523. https://doi.org/10.2217/bmm-2019-0410
62. Wodsedalek DJ, Paddock SJ, Wan TC, Auchampach JA, Kenarsary A, Tsaih SW, Flister MJ, O'Meara CC (2019) IL-13 promotes in vivo neonatal cardiomyocyte cell cycle activity and heart regeneration. Am J Physiol Heart Circ Physiol 316:H24–H34. https://doi.org/10.1152/ajpheart.00521.2018
63. Wu CC, Jeratsch S, Graumann J, Stainier DYR (2020) Modulation of mammalian cardiomyocyte cytokinesis by the extracellular matrix. Circ Res 127:896–907. https://doi.org/10.1161/CIRCRESAHA.119.316303
64. Xin M, Kim Y, Sutherland LB, Murakami M, Qi X, McAnally J, Porrello ER, Mahmoud AI, Tan W, Shelton JM, Richardson JA, Sadek HA, Bassel-Duby R, Olson EN (2013) Hippo pathway effector Yap promotes cardiac regeneration. Proc Natl Acad Sci U S A 110:13839–13844. https://doi.org/10.1073/pnas.1313192110
65. Yousefi K, Irion CI, Takeuchi LM, Ding W, Lambert G, Eisenberg T, Sukkar S, Granzier HL, Methawasin M, Lee DI, Hahn VS, Kass DA, Hatzistergos KE, Hare JM, Webster KA, Shehadeh LA (2019) Osteopontin promotes left ventricular diastolic dysfunction through a mitochondrial pathway. J Am Coll Cardiol 73:2705–2718. https://doi.org/10.1016/j.jacc.2019.02.074
66. Zhang Y, Xia H, Ge X, Chen Q, Yuan D, Chen Q, Leng W, Chen L, Tang Q, Bi F (2014) CD44 acts through RhoA to regulate YAP signaling. Cell Signal 26:2504–2513. https://doi.org/10.1016/j.cellsig.2014.07.031
67. Zhao B, Tumaneng K, Guan KL (2011) The Hippo pathway in organ size control, tissue regeneration and stem cell self-renewal. Nat Cell Biol 13:877–883. https://doi.org/10.1038/ncb2303
68. Zhou Q, Li L, Zhao B, Guan KL (2015) The hippo pathway in heart development, regeneration, and diseases. Circ Res 116:1431–1447. https://doi.org/10.1161/CIRCRESAHA.116.303311